Cell, Vol. 119, 355–368, October 29, 2004, Copyright ©2004 by Cell Press

Homologous Recombination Generates T-Loop-Sized Deletions at Human Telomeres

Richard C. Wang,[1] Agata Smogorzewska,[1,2] and Titia de Lange[1,*]
[1]Laboratory for Cell Biology and Genetics
The Rockefeller University
1230 York Avenue
New York, New York 10021

Summary

The t-loop structure of mammalian telomeres is thought to repress nonhomologous end joining (NHEJ) at natural chromosome ends. Telomere NHEJ occurs upon loss of TRF2, a telomeric protein implicated in t-loop formation. Here we describe a mutant allele of TRF2, TRF2$^{\Delta B}$, that suppressed NHEJ but induced catastrophic deletions of telomeric DNA. The deletion events were stochastic and occurred rapidly, generating dramatically shortened telomeres that were accompanied by a DNA damage response and induction of senescence. TRF2$^{\Delta B}$-induced deletions depended on XRCC3, a protein implicated in Holliday junction resolution, and created t-loop-sized telomeric circles. These telomeric circles were also detected in unperturbed cells and suggested that t-loop deletion by homologous recombination (HR) might contribute to telomere attrition. Human ALT cells had abundant telomeric circles, pointing to frequent t-loop HR events that could promote rolling circle replication of telomeres in the absence of telomerase. These findings show that t-loop deletion by HR influences the integrity and dynamics of mammalian telomeres.

Introduction

Changes in the length of human telomeres are relevant to cancer and aging. Telomere attrition represents a tumor suppressor pathway that limits the replicative potential of potential cancer cells. The gradual loss of telomeric DNA with each round of DNA replication depletes the telomere reserve and leads to a growth arrest that is accompanied by senescence or apoptosis. Most human tumors need to bypass this proliferation block to reach a clinically relevant mass. Telomerase activation has surfaced as the main pathway for the escape from telomere-driven senescence or apoptosis, resulting in nearly ubiquitous expression of telomerase during tumorigenesis (Shay and Bacchetti, 1997). Telomerase-independent pathways (ALT) for telomere maintenance are rare in most human cancers but significant in soft tissue sarcomas (Henson et al., 2002). Telomere shortening has also been implicated in the age-related depletion of stem cell compartments and contributes to the aging symptoms of dyskeratosis congenita patients (Marciniak et al., 2000; Mitchell et al., 1999; Vulliamy et al., 2001). Here, we document that HR can delete large segments of telomeric DNA in human and mouse cells and suggest that this pathway has implications for telomere-related disease states.

Telomeres protect chromosome ends from inappropriate DNA repair and prevent activation of DNA damage checkpoints. Telomere protection is achieved through telomerase-mediated maintenance of telomeric repeats, which endow chromosome ends with binding sites for a protective protein complex. Mammalian telomeric TTAGGG repeats bind TRF2, a dimeric DNA binding protein with a key role in telomere protection (de Lange, 2002). Dwindling presence of the TRF2 complex on shortening telomeres is a likely cause of telomere dysfunction (Karlseder et al., 2002). Like telomeres that are depleted of TRF2, shortened telomeres become associated with DNA damage response factors (e.g., 53BP1), forming cytological structures that are referred to as telomere dysfunction induced foci (TIFs) (Bakkenist et al., 2004; d'Adda di Fagagna et al., 2003; Takai et al., 2003). The ATM kinase plays a major role in the telomere damage response and its ability to activate p53 is largely responsible for telomere-driven cell cycle arrest, senescence and/or apoptosis (d'Adda di Fagagna et al., 2003; Herbig et al., 2004; Karlseder et al., 1999; Takai et al., 2003). TRF2 can function as a direct inhibitor of the ATM kinase, and this feature can explain why long telomeres, which contain 10^3–10^4 copies of TRF2, do not activate the DNA damage pathway (Karlseder et al., 2004).

TRF2 is also crucial for the repression of NHEJ at chromosome ends (Bailey et al., 2001; Smogorzewska et al., 2002; van Steensel et al., 1998; Zhu et al., 2003). Frequent telomere fusions occur when TRF2 is displaced from telomeres and in cells with excessive telomere erosion. The ability of TRF2 to protect telomeres from NHEJ can be explained based on the formation of t-loops (Stansel et al., 2001). T-loops sequester the 3′ end of the chromosome through strand invasion of the telomeric overhang into the duplex TTAGGG repeat array (Griffith et al., 1999). This telomeric configuration is observed in purified telomeric DNA from human, mouse, plant, and protozoan origin (Cesare et al., 2003; Griffith et al., 1999; Munoz-Jordan et al., 2001; Murti and Prescott, 1999) and in native telomeric chromatin from mouse and chicken cells (Nikitina and Woodcock, 2004). When telomeres are in the t-loop configuration, the NHEJ repair machinery may simply not have access to chromosome ends, explaining the resistance of telomeres to fusion. However, t-loops resemble an intermediate in homologous recombination, potentially providing a substrate for their deletion through this pathway (discussed in de Lange [2004], de Lange and Petrini [2000], and Griffith et al. [1999]). Using a mutant allele of TRF2, we show that HR can delete t-loop-sized telomeric segments resulting in rapid shortening of telomeres and generation of extrachromosomal telomeric circles. In addition, we identify circular t-loop HR prod-

*Correspondence: delange@mail.rockefeller.edu
[2]Present address: Department of Pathology, Massachusetts General Hospital, 55 Fruit Street, WRN 219, Boston, Massachusetts 02114.

ucts in normal human cells and ALT cells, providing evidence for the importance of HR in telomere dynamics.

Results

TRF2$^{\Delta B}$: Induction of TIFs and Senescence without Telomere Fusions

TRF2 has a C-terminal Myb-type DNA domain and a TRFH domain that mediates dimerization (Broccoli et al., 1997; Fairall et al., 2001). These domains are very similar to those of TRF1 and Taz1, the TRF1/2 ortholog of *Schizosaccharomyces pombe*. TRF2 is unique in its N terminus, which is comprised of a short segment of basic amino acids. Deletion of this basic domain of TRF2 (TRF2$^{\Delta B}$) does not impede the DNA binding activity of TRF2 (M. van Breughel and T.d.L., unpublished data) or abrogate its ability to promote t-loop formation in vitro (R. Stansel, T.d.L., and J.W. Griffith, unpublished data). TRF2$^{\Delta B}$ localizes to telomeres in vivo (van Steensel et al., 1998) and can bind hRap1 (Li et al., 2000), and overexpression of this allele does not diminish the presence of the Mre11 complex or ERCC1/XPF in the TRF2 complex (Zhu et al., 2000, 2003). In agreement with these findings, telomeric ChIP on cells expressing TRF2$^{\Delta B}$ revealed that the telomeres retained TRF2, TRF1, hRap1, and Mre11 (see Supplemental Figure S1 at http://www.cell.com/cgi/content/full/119/3/355/DC1/).

Despite its apparent proficiency as a telomere binding protein, TRF2$^{\Delta B}$ induced a cell cycle arrest in human fibrosarcoma cells, suggesting that this allele created a defect in telomere function (van Steensel et al., 1998). In addition, TRF2$^{\Delta B}$ resulted in senescence in primary fibroblasts, as indicated by growth arrest, morphological changes, a gradual drop in BrdU incorporation, expression of senescence-associated (SA-) β-galactosidase (Dimri et al., 1995), and a pattern of p53, p16, p21, and pRB expression typical of senescent cells (Figures 1A–1D). TRF2$^{\Delta B}$-expressing cells also developed 53BP1 foci, some of which colocalized with TRF1, a marker for telomeres (Figure 1E). Such sites of colocalization of DNA damage factors and telomeres (TIFs) are indicative of dysfunctional telomeres. However, the TIFs were notably larger and less frequent than in cells expressing the dominant-negative allele of TRF2 (TRF2$^{\Delta B\Delta M}$) (Figure 1E). Furthermore, whereas TRF2$^{\Delta B\Delta M}$ results in telomere fusions mediated by NHEJ, TRF2$^{\Delta B}$ did not have this phenotype (van Steensel et al. [1998] and see below), suggesting that the telomere dysfunction induced by TRF2$^{\Delta B}$ was fundamentally distinct.

TRF2$^{\Delta B}$-Induced Telomere Shortening

Analysis of genomic DNA showed that expression of TRF2$^{\Delta B}$ induced sudden shortening of the telomeric restriction fragments (Figure 2A). Inspection of denatured telomeric restriction fragments on alkaline gels indicated that both the C-rich and the G-rich strands became shortened upon the expression of TRF2$^{\Delta B}$ (Figure 2B). While the loss of telomeric DNA involved the duplex part of the telomere, the G strand overhang signal did not diminish or even increased (Figure 2A and data not shown). This phenotype is clearly distinct from that of TRF2$^{\Delta B\Delta M}$ or TRF2 gene deletion, which leads to a reduction of the G strand overhang signal but preservation of the duplex part of the telomere (van Steensel et al., 1998; G. Celli and T.d.L., unpublished data).

The TRF2$^{\Delta B}$-induced reduction in mean telomere length occurred in a variety of human cell lines (IMR90, WI-38, HS68, BJ/hTERT, HT1080, and HeLa cells) (Figure 2C and data not shown). The change in the TTAGGG repeat signals was quantified using equally loaded gels and hybridization to chromosome internal control fragments to normalize the signals (see Supplemental Figure S2 on the *Cell* web site). The quantitative analysis showed that ~15%–25% of the telomeric DNA was lost in human and mouse cell lines infected with TRF2$^{\Delta B}$. The loss of TTAGGG repeats was roughly proportional to the length of the telomeres, such that longer telomeres lost larger segments of TTAGGG repeats. For instance, mouse cells with telomeres in the 30–50 kb range lost approximately the same fraction of their TTAGGG repeats as did human cells with telomeres in the 5–10 kb range (Figures 2C and D). The loss of telomeric DNA was rapid and occurred at a rate that far exceeds the rate of telomere attrition in telomerase-deficient cells.

TRF2$^{\Delta B}$ Induces Large Stochastic Postreplicative Telomere Deletions

The loss of telomeric sequences was readily detectable using telomere-specific fluorescence in situ hybridization (FISH). Metaphase spreads of mouse and human fibroblasts showed an obvious overall loss in the strength of telomeric FISH signals (Figures 3A and 3B). The telomere deletions did not appear to affect all chromatids equally. While some telomeres appeared relatively unaffected, others were lost completely. Scoring metaphases from several independent infections indicated that TRF2$^{\Delta B}$ expression results in an ~10-fold increase in the number of chromatids lacking detectable telomere signals in several human and mouse cell lines (Supplemental Table S2). Although it is likely that signal-free ends still contain short stretches of telomeric DNA, the data showed that the telomere signal loss is stochastic and due to large deletions in individual telomeres. Metaphase spreads harvested within a few days after introduction of TRF2$^{\Delta B}$ also showed that telomere loss was not random with regard to sister telomeres. Although many chromosomes lost more than one telomere, it was rare for both sister telomeres to lose their signal (Figures 3A and 3B, Supplemental Table S2). This implied that the deletions occurred after the replication of telomeres.

Preferential Deletion of Telomeres Replicated by Leading Strand DNA Synthesis

Inspection of the telomeric signal loss in TRF2$^{\Delta B}$-expressing cells revealed that, on chromosomes with two deleted telomeres, the remaining signals were very often diagonally positioned (Figure 3B). This finding suggested that the telomere deletions might differentially affect telomeres generated by leading and lagging strand DNA synthesis (referred to as leading strand and lagging strand telomeres). Chromosome orientation (CO)-FISH (Bailey et al., 1996) can be used to determine whether a sister telomere is generated by leading or lagging strand DNA synthesis (see Supplemental Figure S3A for

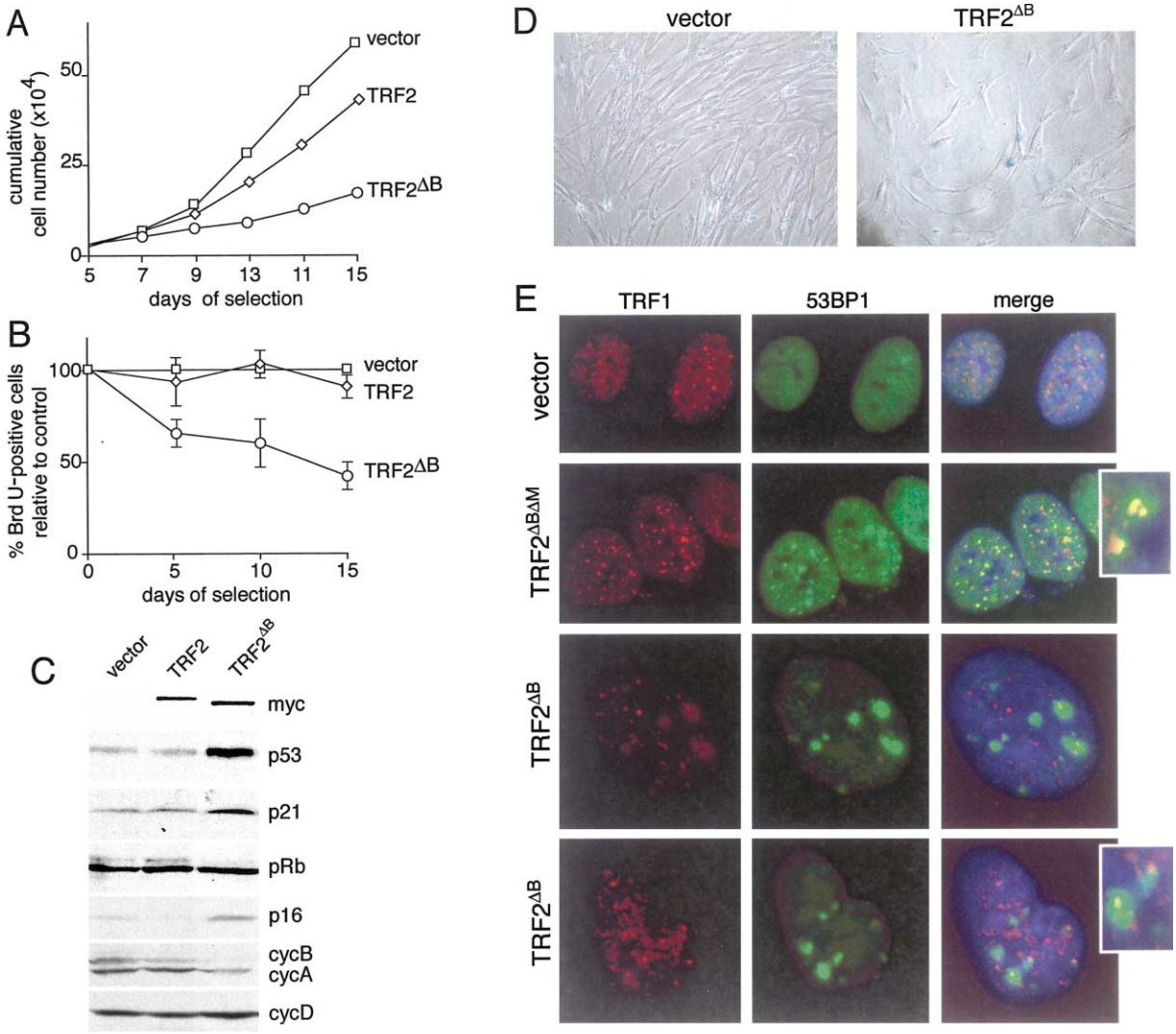

Figure 1. Induction of Senescence and TIFs by TRF2$^{\Delta B}$

(A) Growth curves of IMR90 cells infected with the indicated retroviruses.

(B) Changes in BrdU incorporation of the cultures in (A). BrdU incorporation of vector control cells is set at 100% at day 0; the values represent the mean of 4–5 experiments, and the SD is given. Method as described previously (Smogorzewska and de Lange, 2002).

(C) Immunoblot analysis of IMR90 cells expressing TRF2, TRF2$^{\Delta B}$, and vector control at day 14 of selection.

(D) TRF2$^{\Delta B}$-induced senescent morphology and SA-β-gal expression. WI38 cells infected with the indicated virus stained for SA-β-gal activity at day 10 after selection.

(E) TIFs in BJ/hTERT infected for one day with the indicated viruses. DAPI (blue), 53BP1 IF (green), TRF1 IF (red). Enlarged images show 53BP1 foci at telomeres. Not all TRF2$^{\Delta B}$-induced 53BP1 foci coincided with detectable TRF1 signals.

schematic). Using CO-FISH on controls cells and cells infected with TRF2$^{\Delta B}$, we usually found two diagonally positioned lagging strand telomere signals per chromosome, indicating that the lagging strand telomere remained relatively intact (Supplemental Figure S3B). By scoring the signals on 700 chromosomes from control cells and TRF2$^{\Delta B}$ cells, we found that the number of lagging strand telomeres per chromosome remained constant (2.1 in the vector control and 2.2 after TRF2$^{\Delta B}$ expression; n = 700 chromosomes for each group). In contrast, CO-FISH to detect the leading strand telomeres showed dramatic signal loss after TRF2$^{\Delta B}$ expression (Supplemental Figure S3C). Metaphase chromosomes often contained only one or no leading strand CO-FISH signal. Overall, the leading strand signals per chromosome was 0.74 after TRF2$^{\Delta B}$ expression compared to 1.9 in the vector control (n = 650 chromosomes for each group).

We next visualized both leading and lagging strand telomeres on the same metaphase using CO-FISH (Figure 3C). Control metaphases possessed the expected pattern of two different CO-FISH signals on each pair of sister telomeres. However, metaphases from TRF2$^{\Delta B}$-expressing cells showed a strong leading/lagging strand signal imbalance with far fewer leading strand telomere signals than expected. We conclude that TRF2$^{\Delta B}$ expression results in a preferential deletion of leading strand telomeres after telomere replication. Since sister asym-

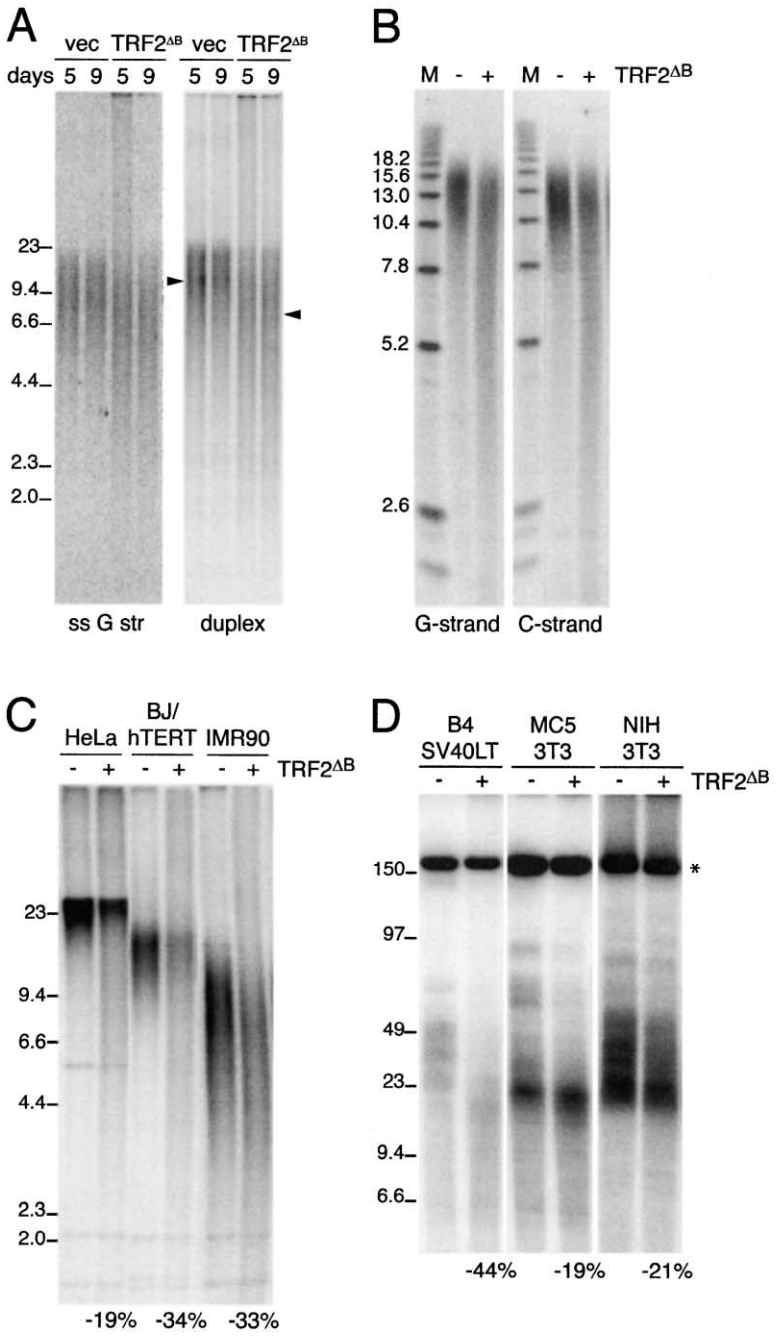

Figure 2. TRF2$^{\Delta B}$ Results in the Loss of Duplex Telomeric DNA but Not G Overhangs in Human and Mouse Cells

(A) TRF2$^{\Delta B}$-induced shortening of the duplex part of the telomere. BJ fibroblasts were harvested at the indicated time points after selection for infection with vector (−) or TRF2$^{\Delta B}$ retrovirus. Equal amounts of MboI- and AluI-digested genomic DNA were fractionated and first probed with end-labeled $(CCCTAA)_4$ under native conditions (left), followed by in situ denaturation of the DNA in the gel and reprobing with the same probe (right). Position and MWs (kb) of λ × HindIII fragments are indicated to the left. Arrowheads indicate approximate median telomere restriction fragment lengths.

(B) Denaturing gel electrophoresis analysis of C and G strand length after expression of TRF2$^{\Delta B}$. BJ/hTERT:SV40LT fibroblasts were harvested on day 10 of selection for infection with vector (−) or TRF2$^{\Delta B}$ (+). Equal amounts of MboI- and AluI-digested genomic DNA were denatured and fractionated on an alkaline gel. After neutralization and blotting, the DNA was probed with labeled $(CCCTAA)_4$ and, after removal of signal, reprobed with $(TTAGGG)_4$. The marker is a self-ligated ladder of a HindIII cut 2.6 kb plasmid containing TTAGGG repeats (pTH5). MWs in kilobases (kb).

(C) TRF2$^{\Delta B}$-induced telomere shortening in HeLa, BJ/hTERT, and IMR90. Telomere blots of MboI- and AluI-digested genomic DNA (from cells on day 4 of selection). Duplex TTAGGG repeat signals were quantified as shown in Supplemental Figure S2.

(D) TRF2$^{\Delta B}$-induced telomere shortening in mouse cells. Genomic DNAs harvested 5 days after infection with vector (−) or TRF2$^{\Delta B}$ retrovirus (+), digested with HindIII, and separated on a CHEF gel. Telomeric signal were quantified as in Supplemental Figure S2. The band at 150 kb (*) presumably represents telomeres with subtelomeric sequences lacking HindIII sites.

metry is erased after each round of DNA replication, the preferential deletion of leading strand telomeres is primarily observed in the first mitosis after TRF2$^{\Delta B}$ has its effect.

TRF2$^{\Delta B}$-Induced Deletions Depend on XRCC3 and NBS1

Since the telomere deletions involved stochastic loss of large segments of telomeric DNA from individual telomeres, we considered that they could be due to homologous recombination at the base of the t-loop. In order to address the contribution of HR to telomere deletions, we determined the effect of TRF2$^{\Delta B}$ in cells with impaired function of XRCC3, a RAD51 paralog that forms a complex with RAD51C (Liu et al., 2004). Although XRCC3 has been implicated in both early and late stages of homologous recombination (Brenneman et al., 2002; Pierce et al., 1999), recent studies have demonstrated that XRCC3 and RAD51C are associated with Holliday junction (HJ) resolvase activity in vitro (Liu et al., 2004). Human HCT116 colon carcinoma cells in which both copies of the XRCC3 gene were inactivated by gene targeting (Yoshihara et al., 2004) were infected with TRF2$^{\Delta B}$ and examined for telomere deletions by quantitative genomic blotting (Figures 4A–4C). DNAs were digested with EcoRI/XbaI and first probed with a chromo-

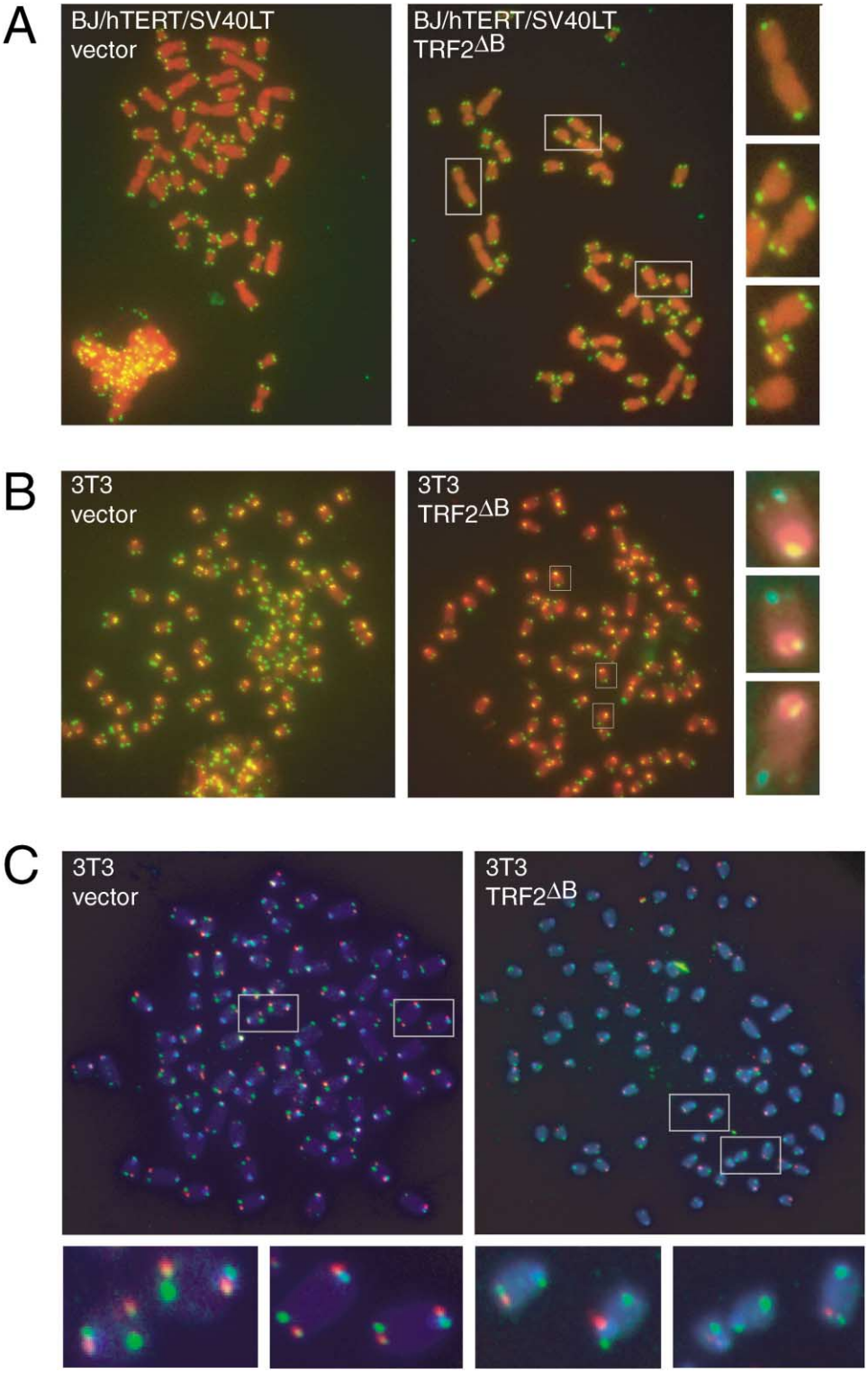

Figure 3. TRF2$^{\Delta B}$-Induced Telomere Deletions Are Stochastic and Preferentially Affect Leading Strand Telomeres

(A) Telomeric FISH on human BJ/hTERT:SV40LT metaphase chromosomes. Infected cells were harvested on day 6 after selection. Enlarged images show chromosomes that lost two individual sister telomeres in an antiparallel fashion.

(B) Telomeric FISH on metaphase spreads from mouse NIH/3T3 cells. Infected cells were harvested 1 day after infection (no selection). Enlarged images show chromosomes with unequal sister signals at both ends.

(C) Preferential deletion of leading strand telomeres detected by CO-FISH. Metaphases harvested from NIH/3T3 mouse cells incubated with BrdU/BrdC were treated to remove the newly synthesized DNA strand. The remaining telomeric DNA strands were detected with TAMRA-$(TTAGGG)_3$ (red) and FITC-$(CCCTAA)_3$ probe (green). The telomere replicated by leading strand synthesis is highlighted in red, and the telomere replicated by lagging strand synthesis is highlighted in green. See Supplemental Figure S3 for CO-FISH schematic.

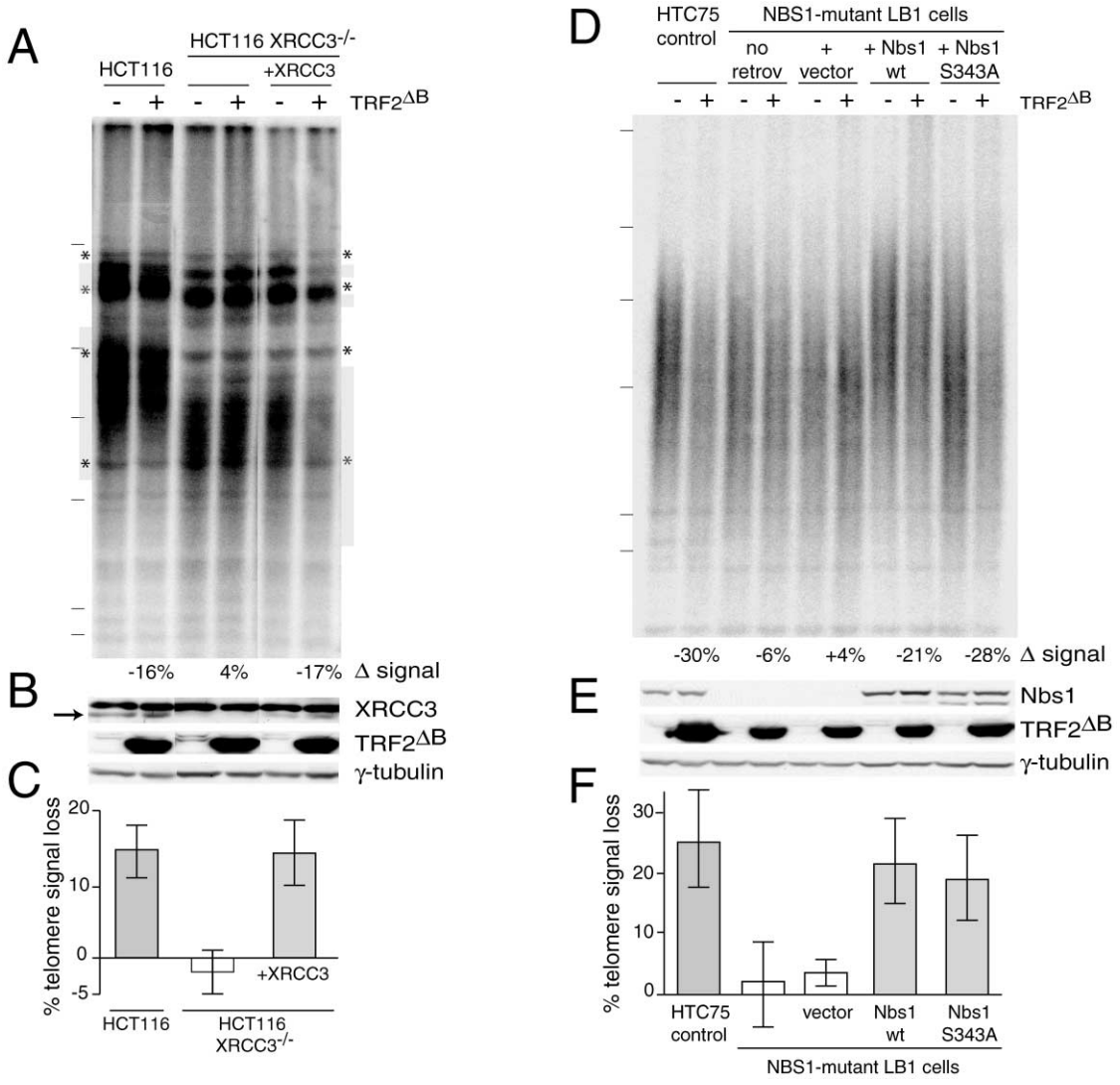

Figure 4. XRCC3 and NBS1 Are Required for TRF2$^{\Delta B}$-Induced Telomere Loss

(A) Requirement for XRCC3. Telomeric signals in human HCT116 cells, XRCC3$^{-/-}$ HCT116 cells, and XRCC3$^{-/-}$ HCT116 cells expressing XRCC3 from exogenous cDNA infected with TRF2$^{\Delta B}$ retrovirus or a vector control and harvested on day 5 after selection. EcoRI- and XbaI-digested DNA was probed for a chromosome-internal locus, quantified, and reprobed for telomeric repeats (shown), and telomere signal loss was quantified as shown in Supplemental Figure S2. A subset of chromosome internal EcoRI and XbaI bands that crosshybridize with telomeric probes are indicated with asterisks. The approximate positions of telomeric signals are indicated with gray boxes next to the lanes.

(B) Immunoblots for XRCC3, TRF2, and γ-tubulin. XRCC3 (arrow) migrates just below a nonspecific band.

(C) Graph showing the effect of XRCC3 deficiency on telomere signal loss. Bars indicate mean loss of telomeric signals (±SD) induced by TRF2$^{\Delta B}$ from five independent genomic preps (three independent infections).

(D) Requirement for NBS1. Human NBS1-LB1 cells were complemented with stable expression of wt Nbs1, Nbs1 S343A, or vector control using pLPC retroviruses. HTC75 fibrosarcoma cells, and NBS1-LB1 cells and their derivatives, were then infected with TRF2$^{\Delta B}$ or the vector control and harvested on day 5 after selection to prepare DNA and protein. Genomic DNA was digested with MboI and AluI, and telomeric signals were quantified. The HTC75 and NBS1-LB1 cells were infected with TRF2$^{\Delta B}$ or the vector control using pLPC; NBS1-LB1 derivative lines were infected using pWZL.

(E) Immunoblots for Nbs1, TRF2, and γ-tubulin.

(F) Graph showing the effect of NBS1 status on telomere signal loss. Bars indicate mean loss of telomeric signals (±SD) induced by TRF2$^{\Delta B}$ from four or more independent genomic preparations (four or more independent infections).

some internal histone gene probe to normalize for loading and then reprobed with a telomeric probe (see Supplemental Figure S2 for procedure). Triplicate experiments were used for the quantification of the effect of XRCC3 status of TRF2$^{\Delta B}$-induced deletions. Although the XRCC3$^{-/-}$ cells expressed the same level of TRF2$^{\Delta B}$ as the control cells (Figure 4B), they did not show telomere deletions (Figures 4A and 4C). Expression of XRCC3 from an introduced cDNA restored the telomere deletion phenotype to the same level as the parental HCT116 cells (Figures 4A–4C). Thus, TRF2$^{\Delta B}$-induced telomere deletions required XRCC3, suggesting that HR is involved in these events. A second RAD51 paralog, RAD51D, has not been implicated in HJ resolution (Liu et al., 2004) but is associated with telomeres (Tarsounas et al., 2004). Using mouse cells lacking RAD51D due to

gene targeting, we found that this RAD51 paralog was not required for the TRF2$^{\Delta B}$-induced deletions (Supplemental Table S1).

A series of other genes involved in DNA repair (e.g., WRN helicase) and DNA damage signaling (e.g., ATM) were tested for their contribution to TRF2$^{\Delta B}$-induced deletions (Supplemental Table S1). Among these, the only gene defect that abrogated TRF2$^{\Delta B}$-mediated deletions was a hypomorphic mutation in NBS1 (Figures 4D–4F). The immortalized human NBS1-LB1 cell line lacks normal Nbs1 protein (Figure 4E) and also has a defect in the nuclear localization of the other components of the Mre11 complex (Lee et al., 2003). These cells showed strongly diminished or no telomere deletion upon expression of TRF2$^{\Delta B}$. TRF2$^{\Delta B}$-induced deletions were also abrogated in a primary human cell line deficient for Nbs1 (Supplemental Figure S4). Introduction of wt Nbs1 or an Nbs1 signaling mutant (S343A; Lim et al., 2000) into NBS1-LB1 cells restored the TRF2$^{\Delta B}$-induced telomere deletions to the same level as HTC75 control cells. Thus, Nbs1 and/or its partners in the Mre11 complex are required for telomere deletions after expression of TRF2$^{\Delta B}$.

HR at Telomeres Yields T-Loop-Sized Circular DNAs

We analyzed the telomeric DNA of TRF2$^{\Delta B}$-expressing cells using neutral-neutral 2D gel electrophoresis, which separates telomeric restriction fragments first by size and then by shape (Brewer and Fangman, 1987; Cohen and Lavi, 1996). The 2D telomere blots of HeLa1.2.11 cells expressing TRF2$^{\Delta B}$ showed the expected shortening of the telomeres compared to control cells (Figure 5). In addition, TRF2$^{\Delta B}$ expression generated a new arc of telomeric DNA, whose migration was consistent with that of relaxed, double-stranded circles (Figure 5A). Expression of TRF2$^{\Delta B}$ also induced the formation of this novel arc in BJ/hTERT cells (Figure 5A) and mouse cells (Supplemental Figure S5). These arcs were not induced by overexpression of TRF1 or the dominant-negative allele of TRF2, confirming their specificity for the TRF2$^{\Delta B}$ allele (Figure 5B and data not shown).

The circular structure of the telomeric molecules in the TRF2$^{\Delta B}$-induced arc was confirmed by two approaches. First, the arc comigrated with circularized $\lambda \times$ HindIII DNA fragments (Figure 5B and Supplemental Figure S5). Second, we reasoned that, if the arc represented circles generated by HR within the telomere, they should be devoid of subtelomeric sequences. To test this, genomic DNA was digested with BglII and EcoRI, which results in telomeric fragments carrying a subtelomeric repeat element present at approximately 10% of human chromosome ends (de Lange et al., 1990). Probing 2D gels with the subtelomeric probe did not reveal a circle arc (Figure 5C), whereas reprobing the same gel with TTAGGG repeats revealed the presence of the circle arc as before. This result corroborated the view that the circle arc represents deleted t-loops and also argued against the possibility that the circle arc was due to DNA replication or recombination intermediates that might cause altered migration behavior in the second dimension.

The size distribution of the circular DNAs reflected the size range of the telomeres. For instance, in HeLa1.2.11 cells with telomeres that are up to 25 kb in length, the circle arc extended from 3 to 20 kb (Figure 5). By contrast, IMR90 cells with telomeres in the 6 to 10 kb range yielded circles with a maximal size of only 9 kb (data not shown). This size distribution of the circular DNAs is consistent with the sizes of t-loops gauged from EM analysis (Griffith et al., 1999). The EM data indicate that t-loops have a broad size distribution in each individual cell line but that the mean t-loop size correlates with telomere lengths. Thus, the data are consistent with deletion of t-loop-sized segments from individual telomeres. Due to the limitations of the resolution in the 2D gels, circular products derived from very short telomeres ($<$3 kb) were not detectable as separated circle arcs. This prohibited the analysis of circular products in the XRCC3 and Nbs1 mutant cell lines, which both have very short TTAGGG repeat regions.

Long exposures of 2D gels of BJ/hTERT or HeLa experiments revealed the presence of low amounts of telomeric circles, even in vector control or uninfected cells (Figure 5). The presence of the circle arc in unperturbed cells indicated that circular telomeric DNA was not strictly a result of TRF2$^{\Delta B}$ expression but may also be generated in small amounts by normal telomere metabolism. This finding is consistent with the occurrence of occasional signal free ends in metaphase spreads of control cells (Figure 3C). Previous studies of Hirt supernatant DNA from mammalian cells had also hinted at the presence telomeric sequences among other circular DNAs (Regev et al., 1998).

Telomeric Circles in ALT Cells

Budding yeast strains that lack telomerase can use one of two HR pathways to maintain their telomeres (reviewed in Lundblad [2002]). HR has also been implicated in the ALT pathway(s) that allow certain human cells to maintain telomeres in the absence of telomerase (Bechter et al., 2004; Dunham et al., 2000; Londono-Vallejo et al., 2004). The findings with TRF2$^{\Delta B}$ suggest that HR is normally controlled at telomeres and predict that the ALT phenotype would require derepression or activation of telomeric HR. Therefore, we examined the occurrence of telomeric circles in ALT cell lines by 2D gel analysis (Figure 6). The results showed that five out of six human ALT cell lines (VA13, Saos-2, SUSM-1, U2 OS, and MeT-4A) contained a strong circle arc, whereas GM847 contained a circle arc of more moderate intensity. The circular telomeric DNA in the five ALT cell lines appeared significantly more abundant than in telomerase-positive cells, reaching similar levels as in cells expressing TRF2$^{\Delta B}$. The telomeric circles may explain the occasional detection of extrachromosomal telomeric DNA in ALT cells (Ford et al., 2001; Tokutake et al., 1998). Some of the ALT cell lines also had a prominent second arc that migrated at the position of supercoiled circular DNA (Figure 6), indicating covalently closed circular DNAs that could be supercoiled due to chromatinization.

Discussion

Human and mouse telomeres can occur in a t-loop configuration in which the 3′ single stranded overhang is tucked into the double-stranded telomeric repeat region. Whereas the t-loop could protect telomeres from

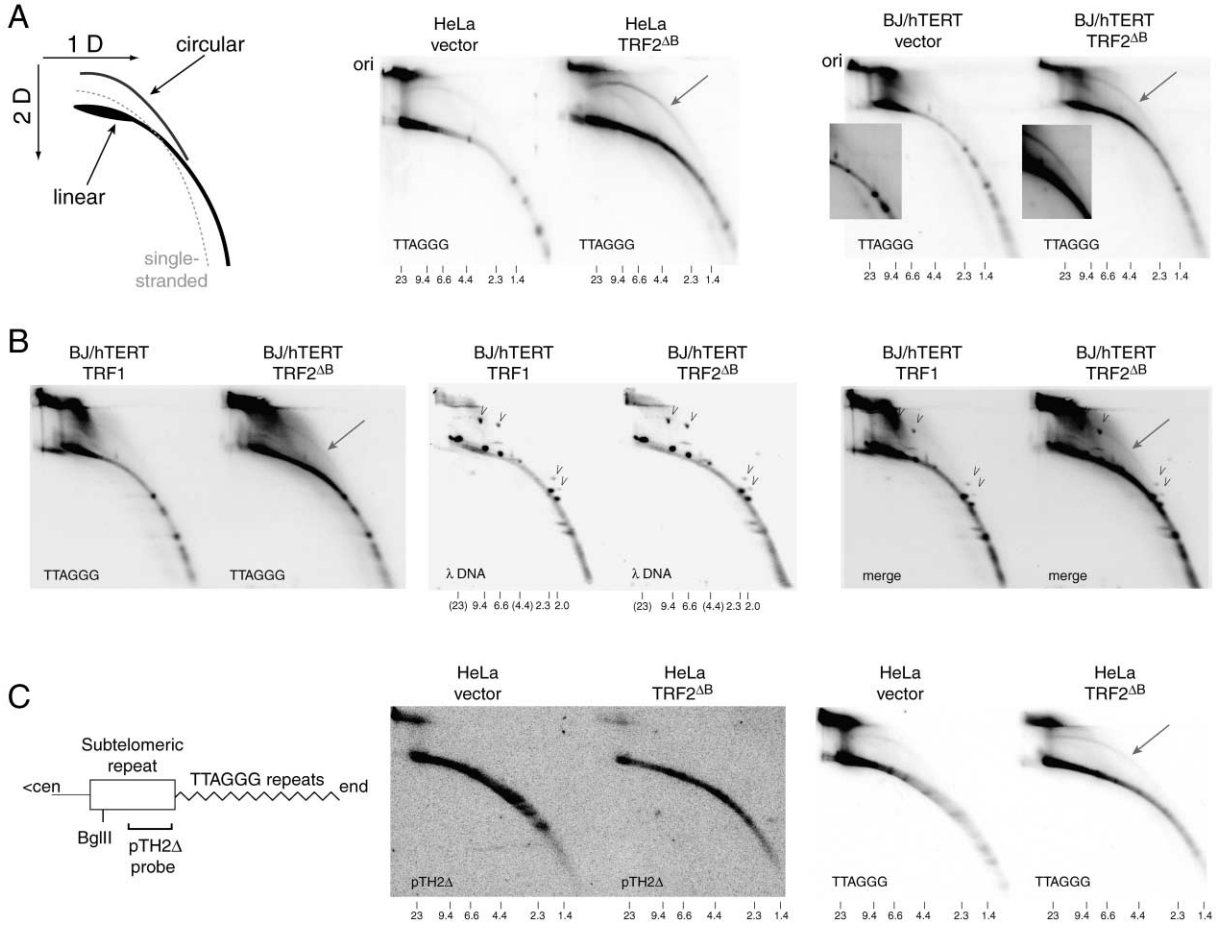

Figure 5. TRF2$^{\Delta B}$-Induced Relaxed Telomeric Circles Detectable by 2D Gels

(A) 2D gel analysis of telomeric DNA from vector control and TRF2$^{\Delta B}$-expressing human cells. (Left) Schematic of the migration of linear dsDNA, ssDNA, and relaxed dsDNA circles (Cohen and Lavi, 1996). DNA from HeLa1.2.11 (middle) and BJ/hTERT (right) cells, infected with the indicated viruses separated by size (1D) and then shape (2D), blotted, and probed for telomeric DNA. MWs in kb. Arrows, telomeric circles induced by TRF2$^{\Delta B}$. Insets, long exposures of part of the blots.

(B) Comigration of circularized λ × HindIII fragments with TRF2$^{\Delta B}$-induced telomeric circles. BJ/hTERT cells were infected with retroviruses expressing TRF1 or TRF2$^{\Delta B}$. Genomic DNA was loaded adjacent to circularized λ × HindIII fragments. The blots were probed for the λ DNA (middle), stripped, and reprobed for telomere repeats (left). The left and middle images were merged in Photoshop (right). Arrowheads, position of circular DNAs. The 23 and 4.4 kb λ × HindIII fragments do not circularize due to their cos ends.

(C) Circular telomeric DNAs are not detected with a subtelomeric probe. (Left) Physical map of a subset of human telomeres that carry the pTH2 subtelomeric repeat element (de Lange et al., 1990). Positions of the probe, subtelomeric repeats, telomeric repeats, and the BglII site are shown. There is no EcoRI site distal from the BglII site. The indicated HeLa DNAs were digested with EcoRI and BglII and probed with pTH2Δ (middle), stripped, and reprobed with a TTAGGG repeat probe.

nonhomologous end joining, it resembles an intermediate in homologous recombination and could therefore be at risk of inappropriate processing by this recombination pathway. The data presented here show that HR is indeed a threat to human telomeres. Telomeres undergo homologous recombination in cells that express a truncated form of the main protective factor at human telomeres, TRF2. Our data show that homologous recombination can delete large segments of telomeric DNA from individual telomeres, generating circular telomeric DNAs of t-loop size presumed to represent detached t-loops. We refer to this process as t-loop HR to distinguish it from homologous recombination between telomeres, a process that could lead to exchange of telomeric DNA but will not lead to net deletion of telomeric DNA. Because telomeric circles are also generated spontaneously in a variety of human cells, we propose that t-loop HR contributes to stochastic shortening of human telomeres.

Telomere NHEJ and T-Loop HR: Double Jeopardy at Chromosome Ends

NHEJ of telomeres is a detrimental event that creates dicentric chromosomes and associated genome instability. At functional telomeres, NHEJ is repressed by TRF2, presumably through formation of t-loops. How telomeres prevent HR and what the consequences are of this repair pathway at natural chromosome ends had not been established. Our data indicate that TRF2 also protects mammalian telomeres from potentially detrimental deletions through t-loop HR.

T-loop HR is enhanced upon introduction of TRF2$^{\Delta B}$, a truncation mutant of TRF2 that lacks the N-terminal basic domain. Unlike the dominant-negative allele of

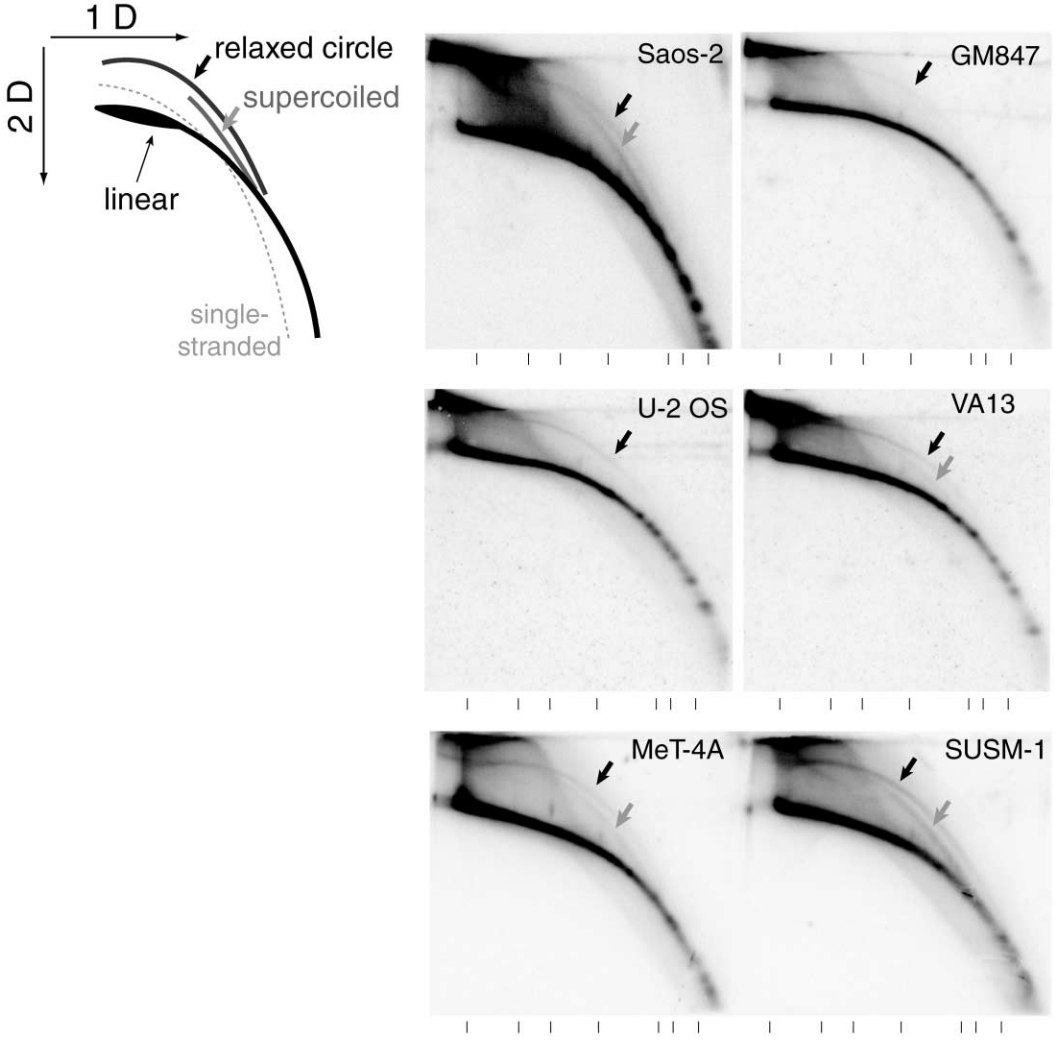

Figure 6. Prominent Telomeric Circle Arcs in ALT Cells

The schematic on the left shows the migration behavior of linear duplex and ssDNA, relaxed circles, and supercoiled circles. The 2D gels show telomeric signals in MboI- and AluI-digested genomic DNA from the indicated human ALT lines. Five out of six lines (not GM847) had elevated levels of circular telomeric DNA (black arrow) when compared to non-ALT cell lines. Four out of six lines (Saos-2, U-2 OS, MeT-4A, and SUSM-1) possessed an additional arc of supercoiled circular telomeric DNA (gray arrow).

TRF2, TRF2$^{\Delta B}$ localizes to telomeres, retains the ability to protect telomeric overhangs from degradation, and blocks NHEJ. However, TRF2$^{\Delta B}$ induced stochastic homologous recombination events at individual telomeres, resulting in deletions and t-loop-sized extrachromosomal circles. The simplest interpretation is that this process of t-loop HR is normally repressed by TRF2 through a mechanism that involves its basic N-terminal domain. Thus, TRF2$^{\Delta B}$ appears to represent a dissociation of function mutant that represses NHEJ but unleashes HR when it displaces (part of) the endogenous TRF2 from telomeres. It is anticipated that the basic domain of TRF2 interacts with one or more other proteins involved in regulation of HR, but the relevant interacting partners are not known at this stage. The ability of TRF2$^{\Delta B}$ to promote HR appears to be specific to telomeres, as levels of sister chromatid exchange (SCE) were comparable between vector control and TRF2$^{\Delta B}$-expressing cells (data not shown).

T-loop HR is not observed upon the expression of TRF2$^{\Delta B\Delta M}$ or when the TRF2 gene is deleted from mouse cells, even when the NHEJ pathway is inactive (Smogorzewska et al., 2002; G. Celli and T.d.L., unpublished data). This suggests that the binding of TRF2 to telomeres is required for efficient t-loop HR. Likely functions for TRF2 in this regard are the formation of t-loops and recruitment of the Mre11 complex, which is implicated in t-loop HR. Both aspects of TRF2 function appear to be unaffected by the deletion of the basic domain in TRF2$^{\Delta B}$. It is not known whether TRF2 affects the efficiency of other types of HR at telomeres (e.g., intertelomeric recombination events). A conserved role for duplex telomere repeat binding proteins in repressing HR at telomeres is consistent with the finding that *S. pombe* can maintain its telomeres through a presumed recombination-based mechanism only when Taz1 is also deleted (Nakamura et al., 1998).

Insight into the control of HR at mammalian telomeres will be important for the understanding of telomere dynamics and may also reveal mechanisms by which HR

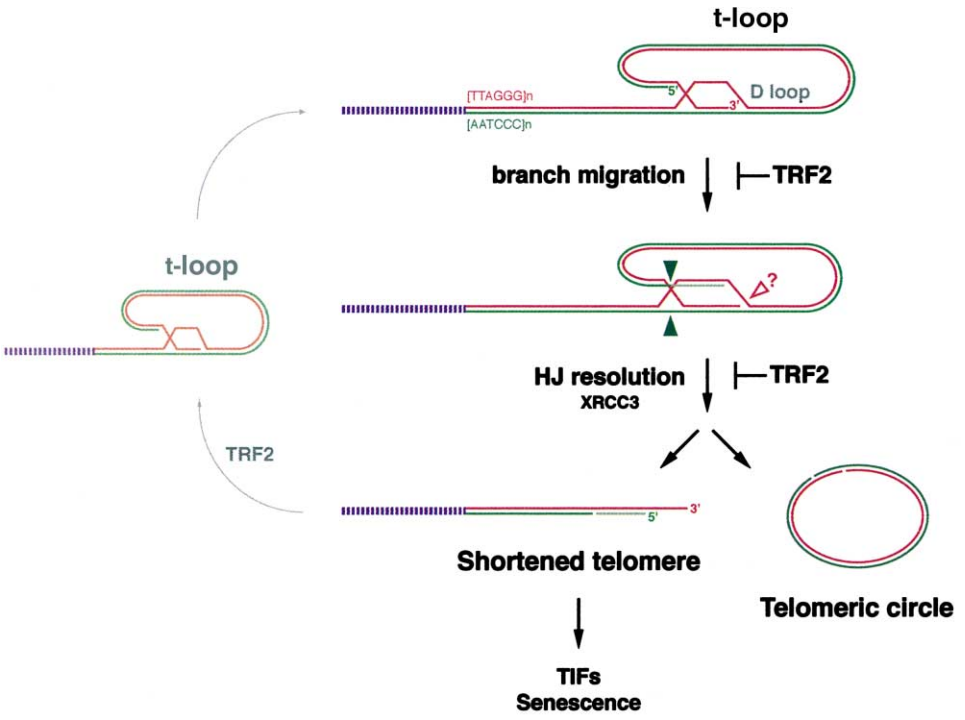

Figure 7. Speculative Model for T-Loop HR

(Top) Proposed structure of t-loops. (Middle) Branch migration at the strand invasion site of the telomere terminus results in the formation of a Holliday junction. (Bottom) Two steps lead to t-loop deletion. Cleavage of the C strand at two positions by HJ resolvase (green arrowheads). This process is proposed to require XRCC3. The second step involves nicking of the D loop by an unknown nuclease (open arrowhead). The products are a shortened telomere and a relaxed telomeric circle. The shortened telomere might reform a small t-loop in a TRF2-dependent manner (left) or, if the deletion is too extensive, might activate a DNA damage response and induce senescence. TRF2 is proposed to promote t-loop formation, thereby creating the substrate for t-loop HR. The basic domain of TRF2 is proposed to suppress t-loop HR by inhibiting branch migration and/or strand cleavage. In ALT cells, the telomeric circles resulting from t-loop HR could function as a template for rolling circle replication and allow telomerase-independent telomere maintenance.

can be controlled. Our analysis of t-loop HR implicates XRCC3, which, together with a second RAD51 paralog, RAD51C, is associated with HJ resolvase activity in vitro (Liu et al., 2004). T-loop HR also required a contribution of the Nbs1 component of the Mre11 complex. The Mre11 complex has been implicated in HR in yeast (Haber, 1998) and chicken DT40 cells (Tauchi et al., 2002). The contribution of the Mre11 complex to mammalian HR has been more difficult to study, since loss of this complex is not compatible with cell viability (Luo et al., 1999). Our results would suggest that Nbs1 and/or other components of the Mre11 complex are required for t-loop HR, but, given the multiplicity of functions ascribed to this complex (Haber, 1998), further analysis is needed to establish the mechanism of its action in this context. The signaling activity of the Mre11 complex is unlikely to be required for t-loop HR, since the signaling-deficient Nbs1 S343A mutation does not abrogate t-loop HR.

Model for T-Loop HR

We propose the following model for t-loop HR (Figure 7). We imagine that the first step is the branch migration of the t-loop invasion site to yield a Holliday junction. This step may not be necessary if the C strand terminus normally invades the internal repeats and a Holliday junction is a permanent feature of (some) T-loops. The EM data on t-loops argue against extensive branch migration but do not exclude the presence of a small segment (<100 bp) of ds telomeric DNA at the t-loop base (Griffith et al., 1999). The second step in t-loop HR is HJ resolution by an activity that involves XRCC3 such that the C strands are cleaved. In order to generate extrachromosomal telomeric circles, a third step, cleavage of the D loop, would be required. The size distribution of telomeric circles formed by this pathway should reflect the size distribution of t-loops, consistent with the 2D gel data. The other product of the reaction is the shortened telomere. This telomere will have a 3′ overhang and may be able to reform a t-loop, albeit a smaller one. Depending on its length, the shortened telomere may be fully functional but could be a substrate for further t-loop HR, eventually leading to a critically shortened telomere that activates the DNA damage response.

Yeast Telomere Rapid Deletions and Mammalian T-Loop HR

The pioneering work of Lustig and colleagues has shown that overelongated yeast telomeres can undergo rapid deletions that reset telomeres to wild-type size (Bucholc et al., 2001; Li and Lustig, 1996; reviewed in Lustig

[2003]). These so-called TRD (telomere rapid deletion) events have several features in common with the t-loop HR reported here. TRD is due to intratelomeric homologous recombination. Physical mapping of deletions in molecularly marked telomeres suggested a model in which the deletions occur through a t-loop-like intermediate that is resolved by HR to yield the shortened telomere. The structure and fate of the deleted segment has remained unknown, in part because yeast TRD is rare ($<10^{-3}$/telomere/division), prohibiting molecular analysis of the immediate products.

While yeast TRD is enhanced in yKu70Δ strains (Polotnianka et al., 1998), TRF2$^{\Delta B}$-induced t-loop HR was not enhanced in mouse cells lacking DNA-PK components or human cells treated with vanillin, a DNA-PKcs inhibitor (Supplemental Table S1). Further analysis will be required to determine the possible role of DNA-PK in mammalian spontaneous and TRF2$^{\Delta B}$-induced t-loop HR. Another apparent difference is the requirement for Nbs1. Human cells lacking Nbs1 fail to execute TRF2$^{\Delta B}$-induced t-loop HR, whereas TRD is only modestly affected by absence of Xrs2 (Bucholc et al., 2001), the Nbs1-like protein of *S. cerevisiae*. However, deficiency in the other components of the Mre11 complex, Mre11 and Rad50, abrogate TRD, stressing a parallel between the mammalian and yeast pathways. Nbs1 mutations in human cells may be more detrimental to the Mre11 complex than lack of Xrs2, perhaps because the nuclear localization of the Mre11 complex is impeded when Nbs1 is not fully functional. Collectively, the data support the view that yeast TRD is a good model for mammalian t-loop HR (Lustig, 2003). Yeast TRD counteracts excessive elongation of telomeres and thus contributes to the maintenance of normal telomere function. It is not unlikely that HR at mammalian telomeres also serves a function in normal telomere metabolism and that t-loop HR only becomes a threat to telomeres when control over this process is lost. This would be consistent with the slight alterations in telomere function observed in mouse cells deficient for RAD54 or RAD51D (Jaco et al., 2003; Tarsounas et al., 2004).

Possible Contribution of T-Loop HR to Telomere Attrition

The most detailed insight in telomere attrition derives from the work of Kipling and colleagues, who examined the length distribution of individual telomeres in clonal telomerase-negative fibroblasts (Baird et al., 2003). Their data show gradual progressive telomere erosion with cell proliferation as well as stochastic changes in telomere length. The latter include telomere deletions with a size range consistent with t-loop deletion. Such sudden deletions can explain the kinetics of senescence in primary human cell strains (Rubelj and Vondracek, 1999). Although telomere erosion is gradual and progressive, affecting all telomeres to the same extent, entry into senescence is not a synchronized event (Smith and Whitney, 1980). Even in a clonal fibroblast line with telomeres of similar initial length, subclones are generated that enter senescence earlier than the bulk of the culture. Telomere length analysis in populations enriched for such early senescent cells showed exaggerated telomere shortening (Martin-Ruiz et al., 2004). T-loop HR could explain these observations. As cells progress through their replicative lifespan, t-loop HR could generate individual cells in which critical telomere shortening arises before general telomere erosion has taken its effect in the bulk population. Thus, telomere-driven senescence would be due to a combination of t-loop HR and gradual erosion; early senescent cells would be more likely to suffer from the former; late senescent cells would potentially suffer from both. The prediction of this proposal is that cells deficient for t-loop HR should still senesce but do so in a more synchronized fashion than wild-type fibroblasts, and early senescent subclones should not be formed.

Spontaneous Telomeric Circles in ALT Cells

The telomeric circles are abundant in most ALT cell lines, consistent with the prior proposal that HR contributes to telomere maintenance in these cells (Dunham et al., 2000). Telomeric circles could be used as a template for telomere extension by rolling circle replication, which has been proposed as one of the possible mechanisms for telomerase-independent telomere maintenance (de Lange, 2004; Henson et al., 2002; Natarajan and McEachern, 2002). The predicted product of t-loop HR is a relaxed circle with nicks in both strands (Figure 7), and relaxed circles are observed in 2D gels. Nicked circles will only allow a single round of rolling circle replication, limiting the potential elongation of telomeres, but their sealing by ligation would allow multiple rounds of replication. The supercoiled telomeric circle arcs we observe in some ALT cells may be indicative of this process.

If the ALT pathway enhances HR at telomeres, telomere deletions are likely to be frequent in these cells. This is consistent with early observations on an ALT cell line that showed stochastic telomere deletions at low frequency (Murnane et al., 1994) and also explains why ALT cell lines often contain chromosome ends lacking telomeric signals (Perrem et al., 2001). Critically shortened telomeres formed by t-loop deletion could affect the growth characteristics of the cells. In glioblastoma multiforme, the ALT pathway is associated with a strikingly better prognosis, suggesting a significant growth difference between telomerase-positive tumor cells and those that use ALT (Hakin-Smith et al., 2003). Furthermore, ALT cells have been reported to grow better when telomerase is expressed (Stewart et al., 2002), a result expected if telomerase helps to heal telomeres that have been truncated by HR.

An Additional Function for Human Telomerase: Counteracting Catastrophic Telomere Deletions

Telomerase is generally thought to counteract the gradual progressive erosion of telomeres, which requires synthesis of up to 200 nt of telomeric DNA per chromosome end per cell division. Counteracting the large deletions generated by t-loop HR is more tasking, requiring the synthesis of up to several kb of telomeric DNA at the affected ends while the other telomeres remain at roughly the same size. This process could explain reports of telomere length-independent functions of telomerase. Telomerase expression has been noted to improve the growth characteristics and telomere function in settings where the enzyme had no detectable

effect on the mean telomere length (e.g., Stewart et al., 2002; Zhu et al., 1999; reviewed in Blackburn [2001]). These findings have been interpreted as evidence for a "capping" function of telomerase. We propose that, in at least some of these experiments, telomerase is required for cell survival because it can repair telomeres deleted by t-loop HR.

A possible role for telomerase in counteracting t-loop HR has implications for telomerase-based cancer therapy. Although telomerase inhibition kills cancer cells, the efficacy of telomerase inhibitors has been debated because of their predicted phenotypic lag (Shay and Wright, 2002). This lag would represent the proliferation needed to deplete the telomere reserve. However, the effect of telomerase inhibition can be remarkably fast in vitro (Hahn et al., 1999). Occasional large telomere deletions through HR can now explain the rapid effect of telomerase inhibition. Cells in which one or more telomeres have undergone t-loop HR and induce a DNA damage response will not proliferate unless telomerase resynthesizes enough telomeric DNA to reconstitute telomere function. Thus, telomerase inhibition may be a fast-acting antitumor strategy in cancers with frequent t-loop HR, and conditions that stimulate t-loop HR could potentially enhance the efficacy of telomerase therapy in the clinic.

Experimental Procedures

2D Gel Electrophoresis and Genomic Blotting

Isolation and digestion of genomic DNA were performed according to standard protocols (Karlseder et al., 2002). For standard telomere blots, MboI- and AluI-digested genomic DNA was fractionated on a 0.7% agarose gel containing 0.1 μg/ml ethidium bromide (EtBr) in 1 $\times$ TAE at $\sim$2V/cm overnight. Neutral-neutral 2D gel electrophoresis was performed according to the protocols established by Brewer and Fangman (http://fangman-brewer.genetics.washington.edu/2Dgel.html/) with the modifications described by Cohen and Lavi (1996).

MEF Preparations and Pulsed-Field Gel Electrophoresis

MEFs were trypsinized, washed once in PBS, and embedded in 1% agarose plugs at a concentration of 1.5 $\times$ 10^6 cells per 100 μl plug. Plugs were incubated in proteinase K digestion buffer (10 mM Tris [pH 7.9], 200 mM EDTA [pH 8.0], 0.2% sodium deoxycholate, 1% sodium lauryl sarcosine, and 500 mg/ml proteinase K; 1 ml per plug) at 50°C overnight (o/n). The plugs were washed extensively in TE (10 mM Tris-HCl [pH 7.5], 1 mM EDTA), equilibrated in digestion buffer for 1 hr, and digested with 120 U of HindIII and 10 μg RNase A in 1 ml for 12 hr. After digestion, plugs were washed in TE and equilibrated in 0.5 $\times$ TBE. The plugs were fractionated on a CHEF-DRII PFGE (Bio-Rad) in a 1% agarose gel in 0.5$\times$ TBE at 6 V/cm for 20 hr at 14°C.

Measurements of Reduction in Telomeric Repeat Signals

Genomic DNA was prepared from cells infected in parallel with vector or TRF2$^{\Delta B}$ retroviruses. After digestion and quantification by Hoechst fluorometry, equal amounts of DNA ($\sim$4 μg) were fractionated, and equal loading was confirmed by EtBr staining. Blots were generally first probed and quantitated for a chromosome internal loading control (see Supplemental Data). The blots were then stripped with boiling 0.1% SDS, rinsed in 2 $\times$ SSC, and hybridized with a TTAGGG repeat probe (pSP73.Sty11; de Lange [1992]), and the telomere signal was quantified in ImageQuant. The telomeric signal was normalized first to the loading control for all lanes; the normalized values for vector- and TRF2$^{\Delta B}$-infected samples were compared and expressed as % signal change in the TRF2$^{\Delta B}$ samples.

Additional technical details and cell culture, viral gene delivery, immunoblotting, ChIP, FISH, and IF procedures are described in Supplemental Data.

Acknowledgments

We are grateful to Kiyoshi Miyagawa, Michael Liskay, John Petrini, Thanos Halazonetis, Paul Hasty, Lexicon Genetics, Fred Alt, Margeret Zdzienicka, Thomas Kunkel, Alan Clark, Winfried Edelman, Hein te Riele, Phillip Smiraldo, and Douglas Pittman for generous gifts of reagents and cell lines. We thank Xu-Dong Zhu, Giulia Celli, Jan Karlseder, Hiro Takai, Diego Loayza, Dirk Hockemeyer, Susan Bailey, and Maria Blasco for invaluable assistance with protocols. Jim Haber and members of the de Lange lab are thanked for helpful discussions and comments on the paper. This work was supported by a grant to T.d.L. from the NIH (GM49046). R.C.W. and A.S. were supported by an NIH MSTP grant (GM07739) to the Cornell/RU/MSK Tri-Institutional MD/PhD program.

Received: July 21, 2004
Revised: September 16, 2004
Accepted: September 28, 2004
Published: October 28, 2004

References

Bailey, S.M., Goodwin, E.H., Meyne, J., and Cornforth, M.N. (1996). CO-FISH reveals inversions associated with isochromosome formation. Mutagenesis *11*, 139–144.

Bailey, S.M., Cornforth, M.N., Kurimasa, A., Chen, D.J., and Goodwin, E.H. (2001). Strand-specific postreplicative processing of mammalian telomeres. Science *293*, 2462–2465.

Baird, D.M., Rowson, J., Wynford-Thomas, D., and Kipling, D. (2003). Extensive allelic variation and ultrashort telomeres in senescent human cells. Nat. Genet. *33*, 203–207.

Bakkenist, C.J., Drissi, R., Wu, J., Kastan, M.B., and Dome, J.S. (2004). Disappearance of the telomere dysfunction-induced stress response in fully senescent cells. Cancer Res. *64*, 3748–3752.

Bechter, O.E., Shay, J.W., and Wright, W.E. (2004). The frequency of homologous recombination in human ALT cells. Cell Cycle *3*, 547–549. Published online May 10, 2004. PMID: 15034305

Blackburn, E.H. (2001). Switching and signaling at the telomere. Cell *106*, 661–673.

Brenneman, M.A., Wagener, B.M., Miller, C.A., Allen, C., and Nickoloff, J.A. (2002). XRCC3 controls the fidelity of homologous recombination: roles for XRCC3 in late stages of recombination. Mol. Cell *10*, 387–395.

Brewer, B.J., and Fangman, W.L. (1987). The localization of replication origins on ARS plasmids in *S. cerevisiae*. Cell *51*, 463–471.

Broccoli, D., Smogorzewska, A., Chong, L., and de Lange, T. (1997). Human telomeres contain two distinct Myb-related proteins, TRF1 and TRF2. Nat. Genet. *17*, 231–235.

Bucholc, M., Park, Y., and Lustig, A.J. (2001). Intrachromatid excision of telomeric DNA as a mechanism for telomere size control in *Saccharomyces cerevisiae*. Mol. Cell. Biol. *21*, 6559–6573.

Cesare, A.J., Quinney, N., Willcox, S., Subramanian, D., and Griffith, J.D. (2003). Telomere looping in *P. sativum* (common garden pea). Plant J. *36*, 271–279.

Cohen, S., and Lavi, S. (1996). Induction of circles of heterogeneous sizes in carcinogen-treated cells: two-dimensional gel analysis of circular DNA molecules. Mol. Cell. Biol. *16*, 2002–2014.

d'Adda di Fagagna, F., Reaper, P.M., Clay-Farrace, L., Fiegler, H., Carr, P., Von Zglinicki, T., Saretzki, G., Carter, N.P., and Jackson, S.P. (2003). A DNA damage checkpoint response in telomere-initiated senescence. Nature *426*, 194–198.

de Lange, T. (1992). Human telomeres are attached to the nuclear matrix. EMBO J. *11*, 717–724.

de Lange, T. (2002). Protection of mammalian telomeres. Oncogene *21*, 532–540.

de Lange, T. (2004). t-loops and the origin of telomeres. Nat. Rev. Mol. Cell Biol. *5*, 323–329.

de Lange, T., and Petrini, J. (2000). A new connection at human telomeres: association of the Mre11 complex with TRF2. Cold Spring Harb. Symp. Quant. Biol. *65*, 265–273.

de Lange, T., Shiue, L., Myers, R.M., Cox, D.R., Naylor, S.L., Killery, A.M., and Varmus, H.E. (1990). Structure and variability of human chromosome ends. Mol. Cell. Biol. *10*, 518–527.

Dimri, G.P., Lee, X., Basile, G., Acosta, M., Scott, G., Roskelley, C., Medrano, E.E., Linskens, M., Rubelj, I., Pereira-Smith, O., et al. (1995). A biomarker that identifies senescent human cells in culture and in aging skin in vivo. Proc. Natl. Acad. Sci. USA *92*, 9363–9367.

Dunham, M.A., Neumann, A.A., Fasching, C.L., and Reddel, R.R. (2000). Telomere maintenance by recombination in human cells. Nat. Genet. *26*, 447–450.

Fairall, L., Chapman, L., Moss, H., de Lange, T., and Rhodes, D. (2001). Structure of the TRFH dimerization domain of the human telomeric proteins TRF1 and TRF2. Mol. Cell *8*, 351–361.

Ford, L.P., Zou, Y., Pongracz, K., Gryaznov, S.M., Shay, J.W., and Wright, W.E. (2001). Telomerase can inhibit the recombination-based pathway of telomere maintenance in human cells. J. Biol. Chem. *276*, 32198–32203.

Griffith, J.D., Comeau, L., Rosenfield, S., Stansel, R.M., Bianchi, A., Moss, H., and de Lange, T. (1999). Mammalian telomeres end in a large duplex loop. Cell *97*, 503–514.

Haber, J.E. (1998). The many interfaces of Mre11. Cell *95*, 583–586.

Hahn, W.C., Stewart, S.A., Brooks, M.W., York, S.G., Eaton, E., Kurachi, A., Beijersbergen, R.L., Knoll, J.H., Meyerson, M., and Weinberg, R.A. (1999). Inhibition of telomerase limits the growth of human cancer cells. Nat. Med. *5*, 1164–1170.

Hakin-Smith, V., Jellinek, D.A., Levy, D., Carroll, T., Teo, M., Timperley, W.R., McKay, M.J., Reddel, R.R., and Royds, J.A. (2003). Alternative lengthening of telomeres and survival in patients with glioblastoma multiforme. Lancet *361*, 836–838.

Henson, J.D., Neumann, A.A., Yeager, T.R., and Reddel, R.R. (2002). Alternative lengthening of telomeres in mammalian cells. Oncogene *21*, 598–610.

Herbig, U., Jobling, W.A., Chen, B.P., Chen, D.J., and Sedivy, J.M. (2004). Telomere shortening triggers senescence of human cells through a pathway involving ATM, p53, and p21(CIP1), but not p16(INK4a). Mol. Cell *14*, 501–513.

Jaco, I., Munoz, P., Goytisolo, F., Wesoly, J., Bailey, S., Taccioli, G., and Blasco, M.A. (2003). Role of mammalian Rad54 in telomere length maintenance. Mol. Cell. Biol. *23*, 5572–5580.

Karlseder, J., Broccoli, D., Dai, Y., Hardy, S., and de Lange, T. (1999). p53- and ATM-dependent apoptosis induced by telomeres lacking TRF2. Science *283*, 1321–1325.

Karlseder, J., Smogorzewska, A., and de Lange, T. (2002). Senescence induced by altered telomere state, not telomere loss. Science *295*, 2446–2449.

Karlseder, J., Hoke, K., Mirzoeva, O.K., Bakkenist, C., Kastan, M.B., Petrini, J.H., and Lange Td, T. (2004). The telomeric protein TRF2 binds the ATM kinase and can inhibit the ATM-dependent DNA damage response. PLoS Biol *2*(8): e240 DOI: 10.1371/journal.pbio.0020240.

Lee, J.H., Xu, B., Lee, C.H., Ahn, J.Y., Song, M.S., Lee, H., Canman, C.E., Lee, J.S., Kastan, M.B., and Lim, D.S. (2003). Distinct functions of Nijmegen breakage syndrome in ataxia telangiectasia mutated-dependent responses to DNA damage. Mol. Cancer Res. *1*, 674–681.

Li, B., and Lustig, A.J. (1996). A novel mechanism for telomere size control in *Saccharomyces cerevisiae*. Genes Dev. *10*, 1310–1326.

Li, B., Oestreich, S., and de Lange, T. (2000). Identification of human Rap1: implications for telomere evolution. Cell *101*, 471–483.

Lim, D.S., Kim, S.T., Xu, B., Maser, R.S., Lin, J., Petrini, J.H., and Kastan, M.B. (2000). ATM phosphorylates p95/nbs1 in an S-phase checkpoint pathway. Nature *404*, 613–617.

Liu, Y., Masson, J.Y., Shah, R., O'Regan, P., and West, S.C. (2004). RAD51C is required for Holliday junction processing in mammalian cells. Science *303*, 243–246.

Londono-Vallejo, J.A., Der-Sarkissian, H., Cazes, L., Bacchetti, S., and Reddel, R.R. (2004). Alternative lengthening of telomeres is characterized by high rates of telomeric exchange. Cancer Res. *64*, 2324–2327.

Lundblad, V. (2002). Telomere maintenance without telomerase. Oncogene *21*, 522–531.

Luo, G., Yao, M.S., Bender, C.F., Mills, M., Bladl, A.R., Bradley, A., and Petrini, J.H. (1999). Disruption of mRad50 causes embryonic stem cell lethality, abnormal embryonic development, and sensitivity to ionizing radiation. Proc. Natl. Acad. Sci. USA *96*, 7376–7381.

Lustig, A.J. (2003). Clues to catastrophic telomere loss in mammals from yeast telomere rapid deletion. Nat. Rev. Genet. *4*, 916–923.

Marciniak, R.A., Johnson, F.B., and Guarente, L. (2000). Dyskeratosis congenita, telomeres and human ageing. Trends Genet. *16*, 193–195.

Martin-Ruiz, C., Saretzki, G., Petrie, J., Ladhoff, J., Jeyapalan, J., Wei, W., Sedivy, J., and Von Zglinicki, T. (2004). Stochastic variation in telomere shortening rate causes heterogeneity of human fibroblast replicative life span. J. Biol. Chem. *279*, 17826–17833.

Mitchell, J.R., Wood, E., and Collins, K. (1999). A telomerase component is defective in the human disease dyskeratosis congenita. Nature *402*, 551–555.

Muñoz-Jordan, J.L., Cross, G.A., de Lange, T., and Griffith, J.D. (2001). t-loops at trypanosome telomeres. EMBO J. *20*, 579–588.

Murnane, J.P., Sabatier, L., Marder, B.A., and Morgan, W.F. (1994). Telomere dynamics in an immortal human cell line. EMBO J. *13*, 4953–4962.

Murti, K.G., and Prescott, D.M. (1999). Telomeres of polytene chromosomes in a ciliated protozoan terminate in duplex DNA loops. Proc. Natl. Acad. Sci. USA *96*, 14436–14439.

Nakamura, T.M., Cooper, J.P., and Cech, T.R. (1998). Two modes of survival of fission yeast without telomerase. Science *282*, 493–496.

Natarajan, S., and McEachern, M.J. (2002). Recombinational telomere elongation promoted by DNA circles. Mol. Cell. Biol. *22*, 4512–4521.

Nikitina, T., and Woodcock, C.L. (2004). Closed chromatin loops at the ends of chromosomes. J. Cell Biol. *166*, 161–165. Published online July 12, 2004. 10.1083/jcb.200403118

Perrem, K., Colgin, L.M., Neumann, A.A., Yeager, T.R., and Reddel, R.R. (2001). Coexistence of alternative lengthening of telomeres and telomerase in hTERT-transfected GM847 cells. Mol. Cell. Biol. *21*, 3862–3875.

Pierce, A.J., Johnson, R.D., Thompson, L.H., and Jasin, M. (1999). XRCC3 promotes homology-directed repair of DNA damage in mammalian cells. Genes Dev. *13*, 2633–2638.

Polotnianka, R.M., Li, J., and Lustig, A.J. (1998). The yeast Ku heterodimer is essential for protection of the telomere against nucleolytic and recombinational activities. Curr. Biol. *8*, 831–834.

Regev, A., Cohen, S., Cohen, E., Bar-Am, I., and Lavi, S. (1998). Telomeric repeats on small polydisperse circular DNA (spcDNA) and genomic instability. Oncogene *17*, 3455–3461.

Rubelj, I., and Vondracek, Z. (1999). Stochastic mechanism of cellular aging—abrupt telomere shortening as a model for stochastic nature of cellular aging. J. Theor. Biol. *197*, 425–438.

Shay, J.W., and Bacchetti, S. (1997). A survey of telomerase activity in human cancer. Eur. J. Cancer *33*, 787–791.

Shay, J.W., and Wright, W.E. (2002). Telomerase: a target for cancer therapeutics. Cancer Cell *2*, 257–265.

Smith, J.R., and Whitney, R.G. (1980). Intraclonal variation in proliferative potential of human diploid fibroblasts: stochastic mechanism for cellular aging. Science *207*, 82–84.

Smogorzewska, A., and de Lange, T. (2002). Different telomere damage signaling pathways in human and mouse cells. EMBO J. *21*, 4338–4348.

Smogorzewska, A., Karlseder, J., Holtgreve-Grez, H., Jauch, A., and de Lange, T. (2002). DNA ligase IV-dependent NHEJ of deprotected mammalian telomeres in G1 and G2. Curr. Biol. *12*, 1635–1644.

Stansel, R.M., de Lange, T., and Griffith, J.D. (2001). T-loop assembly in vitro involves binding of TRF2 near the 3′ telomeric overhang. EMBO J. *20*, E5532–E5540.

Stewart, S.A., Hahn, W.C., O'Connor, B.F., Banner, E.N., Lundberg, A.S., Modha, P., Mizuno, H., Brooks, M.W., Fleming, M., Zimonjic, D.B., et al. (2002). Telomerase contributes to tumorigenesis by a telomere length-independent mechanism. Proc. Natl. Acad. Sci. USA *99*, 12606–12611. Published online August 22, 2002. 10.1073/pnas.182407599

Takai, H., Smogorzewska, A., and de Lange, T. (2003). DNA damage foci at dysfunctional telomeres. Curr. Biol. *13*, 1549–1556.

Tarsounas, M., Munoz, P., Claas, A., Smiraldo, P.G., Pittman, D.L., Blasco, M.A., and West, S.C. (2004). Telomere maintenance requires the RAD51D recombination/repair protein. Cell *117*, 337–347.

Tauchi, H., Kobayashi, J., Morishima, K., van Gent, D.C., Shiraishi, T., Verkaik, N.S., vanHeems, D., Ito, E., Nakamura, A., Sonoda, E., et al. (2002). Nbs1 is essential for DNA repair by homologous recombination in higher vertebrate cells. Nature *420*, 93–98.

Tokutake, Y., Matsumoto, T., Watanabe, T., Maeda, S., Tahara, H., Sakamoto, S., Niida, H., Sugimoto, M., Ide, T., and Furuichi, Y. (1998). Extra-chromosomal telomere repeat DNA in telomerase-negative immortalized cell lines. Biochem. Biophys. Res. Commun. *247*, 765–772.

van Steensel, B., Smogorzewska, A., and de Lange, T. (1998). TRF2 protects human telomeres from end-to-end fusions. Cell *92*, 401–413.

Vulliamy, T., Marrone, A., Goldman, F., Dearlove, A., Bessler, M., Mason, P.J., and Dokal, I. (2001). The RNA component of telomerase is mutated in autosomal dominant dyskeratosis congenita. Nature *413*, 432–435.

Yoshihara, T., Ishida, M., Kinomura, A., Katsura, M., Tsuruga, T., Tashiro, S., Asahara, T., and Miyagawa, K. (2004). XRCC3 deficiency results in a defect in recombination and increased endoreduplication in human cells. EMBO J. *23*, 670–680.

Zhu, J., Wang, H., Bishop, J.M., and Blackburn, E.H. (1999). Telomerase extends the lifespan of virus-transformed human cells without net telomere lengthening. Proc. Natl. Acad. Sci. USA *96*, 3723–3728.

Zhu, X.D., Kuster, B., Mann, M., Petrini, J.H., and de Lange, T. (2000). Cell-cycle-regulated association of RAD50/MRE11/NBS1 with TRF2 and human telomeres. Nat. Genet. *25*, 347–352.

Zhu, X.D., Niedernhofer, L., Kuster, B., Mann, M., Hoeijmakers, J.H., and de Lange, T. (2003). ERCC1/XPF Removes the 3′ overhang from uncapped telomeres and represses formation of telomeric DNA-containing double minute chromosomes. Mol. Cell *12*, 1489–1498.

Note Added in Proof

Cesare and Griffith independently observed circular molecules in ALT cells by electron microscopic analysis of purified telomeric DNA: Cesare, A.J., and Griffith, J.D. (2004). Telomeric DNA in ALT cells is characterized by free telomeric circles and heterogeneous t-loops. Mol. Cell Biol., in press.

Supplemental Data for

Wang et al., Cell 119, pp. 355–368

Supplemental Experimental Procedures

Cell Culture

WI-38 (ATCC), IMR90 (ATCC), GM07166B (Nbs1) (Coriell), AG03141C (WRN) (ATCC), AG04405A (ATM) (ATCC), and AG02496 (ATM) (ATCC) were grown in DMEM with 100 U of penicillin and 0.1 mg of streptomycin, 2 mM L-glutamine, 0.1 mM nonessential amino acids (GIBCO), 1 mM sodium pyruvate (Sigma) and 15% FBS. U-2 OS (ATCC) and Saos-2 (ATCC) were grown in McCoy's 5a medium with supplements and 10% or 15% FBS, respectively. MeT-4A cells were grown in RPMI with 10% FBS. SUSM-1, GM847, VA13, HTC75, HeLaI.2.11, NBS1-LB1 (Kraakman-van der Zwet et al. [1999]; a gift from M. Zdzienicka), Phoenix amphotropic, and Phoenix ecotropic packaging cells were grown in DMEM with supplements and 10% FBS. BJ/hTERT cells (Clontech) were grown according to the manufacturer's specifications. NIH3T3, ERCC1-/- and littermate cells (Zhu et al., 2003), DNA-PKcs-/- (Gao et al. [1998]; a generous gift from F. Alt), Ku86-/-p53-/- and Ku86+/+p53-/- (Zhu et al., 1996), and RAD51-/-p53-/- and RAD51+/+p53-/- (Tarsounas et al. [2004]; a generous gift from D. Pittman) were grown in DMEM with supplements and 10% FBS (or 15% heat inactivated FBS and 50 μM 2-b-mercaptoethanol for primary MEFs). Growth curves, BrdU labeling, and SA-b-galactosidase assays were done as previously described (Smogorzewska and de Lange, 2002). TIF analysis on BJ/hTERT cells was performed as previously described (Takai et al., 2003).

Retroviral Gene Delivery

Either pLPCpuro or pWZLhygro was used as retroviral vectors for expression of TRF2, TRF2ΔB, and TRF1. Primary MEFs were transformed with pBabeNeoSV40largeT at early passage. Retroviral gene delivery was performed as described (Karlseder et al., 2002) except that cells were infected three times at 12 hr intervals. Primary AT fibroblasts (AG04405A, AG02496) were infected three times at 24 hr intervals. Retrovirally infected cells were selected in the appropriate drugs (puromycin 2 μg/ml, hygromycin 90 μg/ml, or G418 600 μg/ml) for 4–5 days until uninfected control cells were completed selected. ERCC1+/+ and ERCC1-/- cells were selected in 3 μg/ml puromycin. Infection of NIH/3T3 cells proved to be very efficient (>90% expression after three rounds). Thus, for better preservation of telomere signals, FISH was performed on NIH/3T3 cells immediately after a 24 hr recovery from two 12 hr infections without selection.

Immunoblotting and Chromatin Immunoprecipitation

Whole-cell lysates were prepared and fractionated as previously described (Smogorzewska and de Lange [2002] and Loayza and De Lange [2003]). For chromatin immunoprecipitation (ChIP), 25 μl of the following crude sera were used: TRF1 (371), TRF2 (647), TRF2 basic domain (508), hRap1 (765), Mre11 (874), Mre11 preimmune (874). For Westerns, the following antibodies were used at the manufacturers' recommended dilutions (except where noted): p53 (DO-1), p21 (Upstate F-5), Rb (Pharmingen 14001A), p16 (Novacastra NCL p16), cyclin A (Santa Cruz sc-239), cyclin D (Santa Cruz), Nbs1 (generous gift from J. Petrini, Hp95 #16/9, 1:20,000), XRCC3 (Chemicon 3776, 5μg/ml), g-tubulin (Sigma GTU88, 1:20,000).

Measurements of Reduction in Telomeric Repeat Signals

Cells were infected with vector or TRF2ΔB retroviruses and processed in parallel. Cells were harvested, and genomic DNA was isolated, digested with the indicated restriction enzymes, and quantified by Hoechst flourometry after digestion. Equal amounts of DNA (4 mg) were fractionated, and equal loading was confirmed by EtBr staining. Blots were generally first probed for a loading control. For human DNA, two control probes were used—a 475 bp Histone H1.3 (PCR primer sequences available upon request) or a fraction of genomic sequences that migrate at ~23 kb after MboI + AluI digestion (referred to as genomic DNA in Supplemental Figure S2) that contains unknown repetitive sequences lacking MboI/AluI sites. The blots were exposed on PhophorImager screens, and the loading control signal was quantified using Imagequant. For mouse DNA, the mTRF2 probe was used as described above, and bands representing the mTRF2 gene were used as loading control. The blots were then stripped with boiling 0.1%SDS, rinsed in 2xSSC, and hybridized with a TTAGGG repeat probe (pSP73.Sty11; de Lange [1992]), and the telomere signal was quantified in Imagequant. The telomeric signal was normalized to the loading control for all lanes, and the normalized values for vector and TRF2ΔB infected samples were compared and expressed as percent signal change in the TRF2ΔB samples.

2D Gel Electrophoresis and Genomic Blotting

Isolation and digestion of genomic DNA were performed according to standard protocols (Karlseder et al., 2002). For standard telomere blots, MboI- and AluI-digested genomic DNA was fractionated on a 0.7% agarose gel containing 0.1 μg/ml ethidium bromide (EtBr) in 1 × TAE at ~2 V/cm overnight. Neutral-neutral 2D gel electrophoresis was performed according to the protocols established by Brewer and Fangman (http://fangman-brewer.genetics.washington.edu/2Dgel.html) with the modifications described by Cohen and Lavi (1996). An equal amount (10–15 μg) of digested genomic DNA was separated on a 0.4% agarose gel in 1 × TBE at 1 V/cm for 20–24 hr. The gel was stained with 0.3 μg EtBr per ml, and lanes were cut, placed orthogonally, and cast in 1.1% agarose in 1 × TBE containing 0.3 μg EtBr per ml. The second dimension was run in at 4–5 V/cm for 3.5 hr at RT. Genomic blotting was performed as previously described (van Steensel and de Lange, 1997). Circularized marker DNA was generated by ligating HindIII-digested I DNA (NEB) at 5 ng/μl overnight at 16°C. The ligated DNA was ethanol precipitated in the presence of glycogen and resuspended at 500 ng/μl; 500 ng was used per lane. To generate the ladder probe, HindIII cut I DNA was digested with BstEII and gel purified. Approximately 2 μg of the digested I DNA was labeled with T4 PNK and g32P-ATP.

Metaphase Chromosome Spreads, FISH, and CO-FISH

Metaphase spreads were prepared as previously described (van Steensel et al., 1998). FISH was performed using a FITC-conjugated PNA probe specific for the G strand (FITC-5¢-[CCCTAA]3-3¢) (Applied Biosystems). CO-FISH was performed using either the FITC-TelC probe or a TAMRA-conjugated PNA probe specific for the C strand (TAMRA-5-[TTAGGG]3-3¢) (Applied Biosystems) essentially as described previously (Bailey et al., 2001) except that cells were grown in the presence of BrdU:C (3:1 ratio, 10 μM total concentration) for 18 hr and incubated in demecolcine (0.1 μg/ml) for the final 2 hr. For simultaneous visualization of both strands, following the standard CO-FISH degradation, both FITC-TelC and TAMRA-TelG probes were added to the hybridization buffer to 0.5 μg/ml. The slides were then denatured at 80°C, hybridized at room temperature, and processed as above.

Supplemental Figures

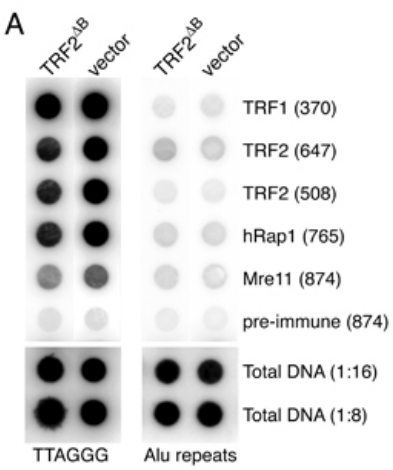

B

Telomeric ChIP quantitation (% TTAGGG repeat signal in ChIP)

Cell line	retrovirus	TRF1	TRF2[b]	TRF2[c]	hRap1	Mre11	PI
HeLa1.2.11	vector	43	14	16	17	4	<1
HeLa1.2.11	TRF2$^{\Delta B}$	43	12	12	12	3	<1

[a] ChIP was performed as described by Loayza and de Lange (2003). Numbers indicate the percentage of total TTAGGG repeat signal recovered in ChIPs with antibodies for the indicated proteins. PI=preimmune serum.
[b] TRF2 ChIP with Ab 647
[c] TRF2 ChIP with Ab 508

Supplemental Figure S1. Telomeric ChIP Monitoring the effect of TRF2ΔB on the Presence of Telomeric Proteins at Chromosome Ends

(A) ChIP on HeLa cells infected with pLPC or pLPC-TRF2ΔB using the indicated antibodies. Duplicate blots were hybridized with a TTAGGG repeats or an Alu repeat probe.

(B) Quantified telomeric ChIP data.

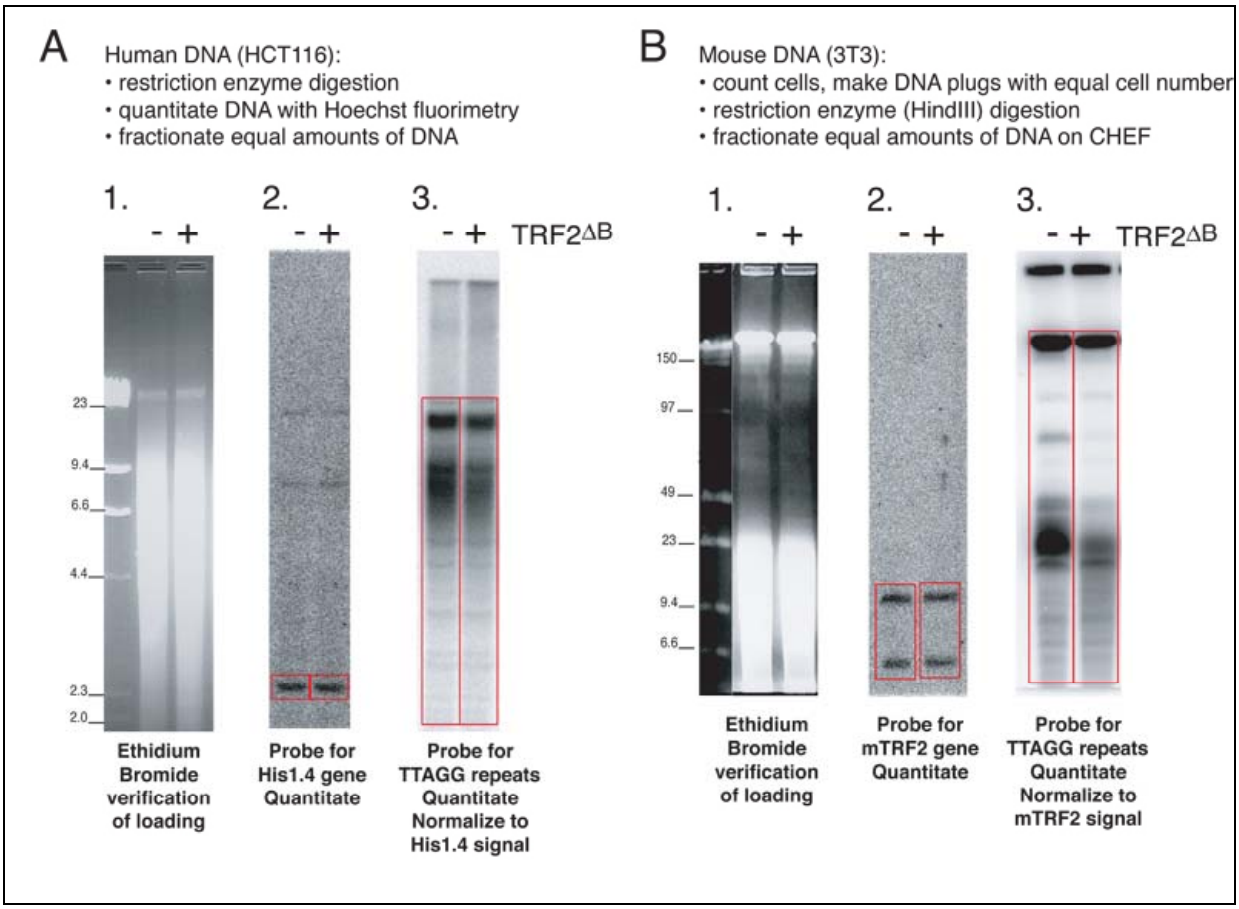

Supplemental Figure S2. Illustration and Examples of Methods Used for Quantification of Telomeric Signal Loss

See Experimental Procedures for further details. The gray boxes indicate the areas in the gels that were quantified. Normalization of human blots with a genomic DNA probe is shown in Supplemental Figure S4.

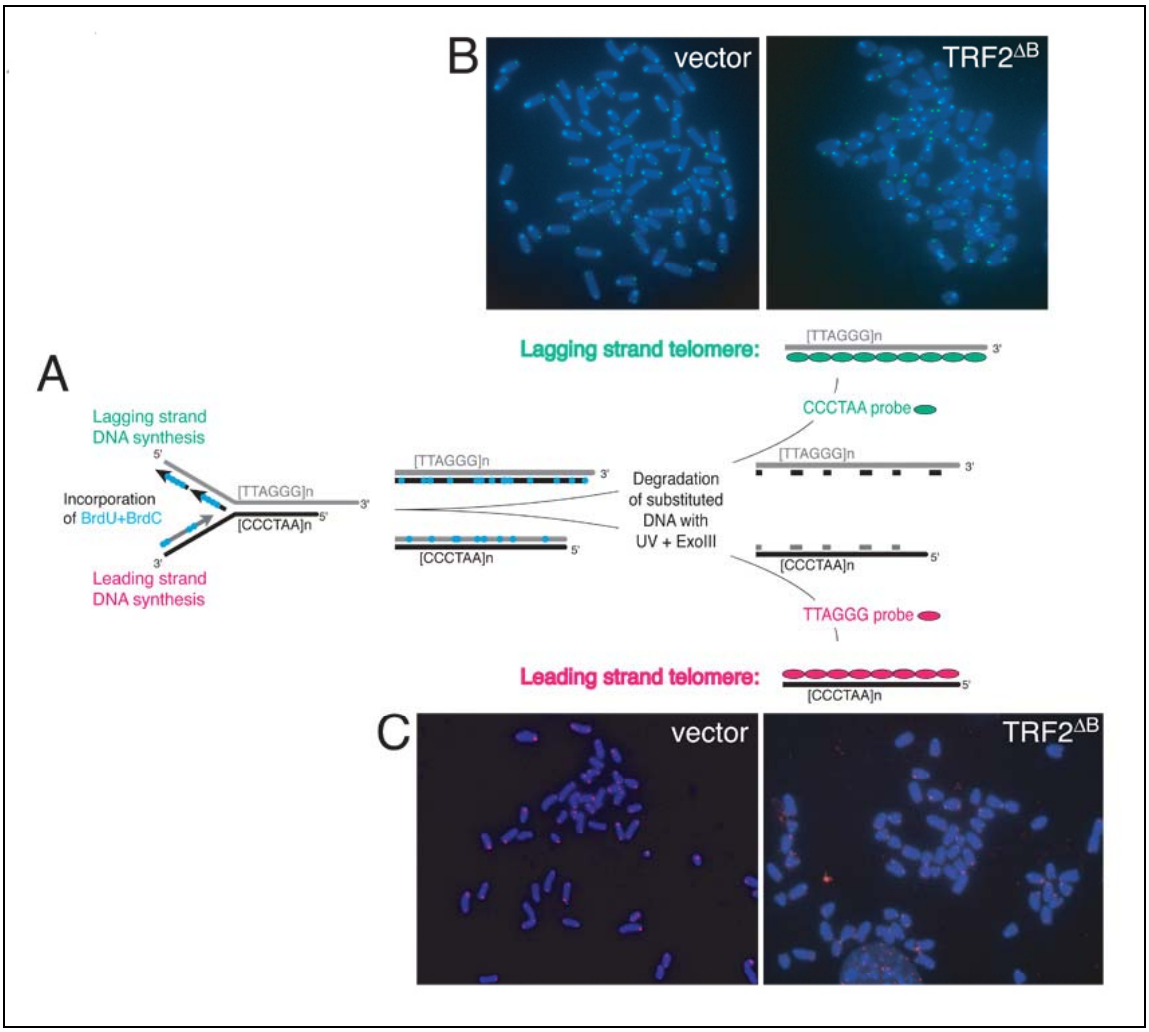

Supplemental Figure S3. Preferential Deletion of Leading Strand Telomeric Signals Detected by CO-FISH

(A) CO-FISH schematic. Cells are grown in the presence of BrdU and BrdC for one S phase. After preparation of metaphase spreads, DNA is treated with UV light, which nicks DNA preferentially at sites of halogenated pyrimidine incorporation. After treatment with ExoIII, the newly synthesized DNA strand is degraded and only parental telomeric sequences remain. The parental strands are then detected with strand-specific FISH.

(B) Lagging strand telomeres are largely preserved in TRF2ΔB-expressing metaphases. Metaphase spreads were prepared from NIH/3T3 cells 48 hr after introduction of vector or TRF2ΔBvirus. The spreads were subjected to CO-FISH and stained with DAPI (red) and a G-rich specific FISH probe FITC-(CCCTAA)3 (green).

(C) Leading strand telomeres are preferentially deleted after TRF2ΔB expression. After metaphases were treated with the CO-FISH protocol, they were stained with DAPI (blue) and a lagging strand specific FISH probe TAMRA-(TTAGGG)3 (red).

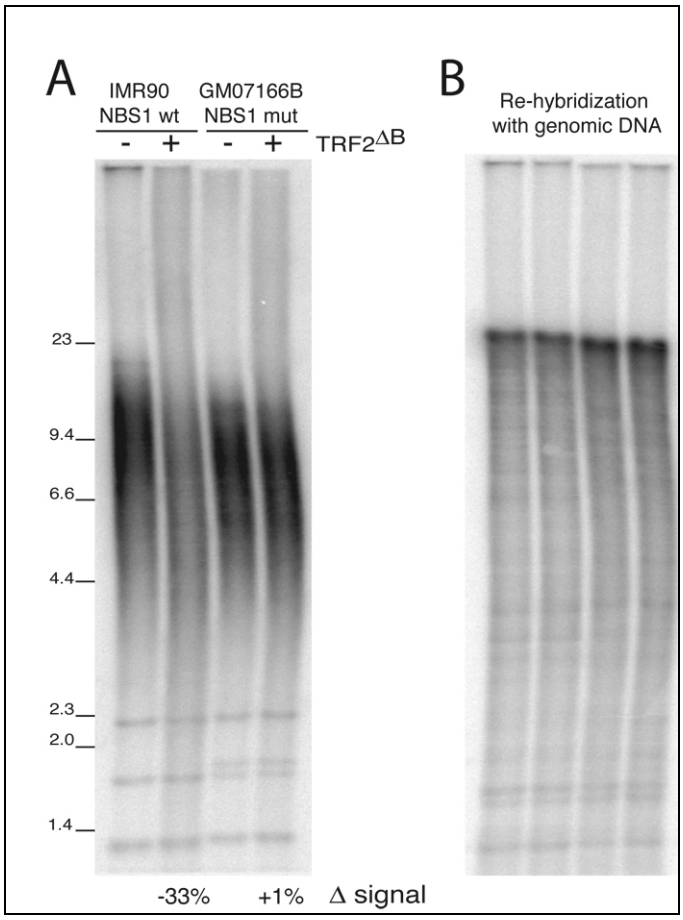

Supplemental Figure S4. Abrogation of TRF2ΔB-Mediated Telomere Deletion in Primary Nbs1 Mutant Fibroblasts

Primary Nbs1 mutant fibroblasts (GM07166B; Coriell) were infected with TRF2ΔB or the vector control and harvested on day 6 after selection to prepare DNA and protein. Absence of Nbs1 protein in Nbs1 fibroblasts and expression of TRF2ΔB were confirmed by immunoblotting (data not shown). Genomic DNA was digested with MboI and AluI and 3 μg (quantitated by Hoechst fluorometry) was fractionated and blotted for telomeric signals (left). The same blot was stripped and reprobed to confirm equal loading using a genomic probe as described in the Experimental Procedures (right). The blots were quantified and normalized using the signal in the right-hand panel for normalization. The numbers below the lane represent the percentage change in telomeric signal intensity relative to the vector control.

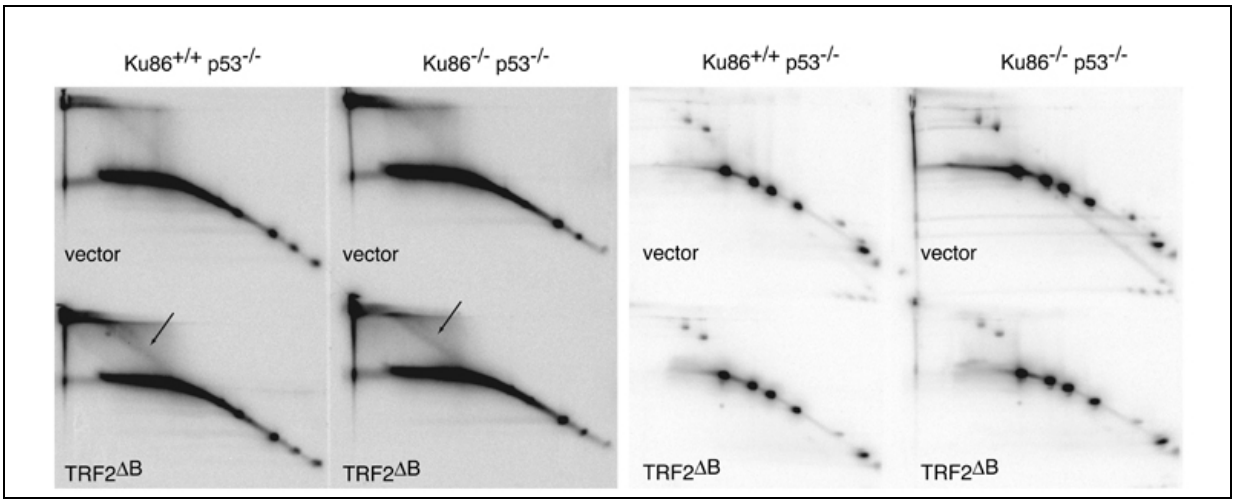

Supplemental Figure S5. TRF2ΔB-Induced Relaxed Telomeric Circles in Mouse Cells Detectable by 2D Gels

MEFs of the indicated genotypes were infected with TRF2ΔB or vector control retroviruses and harvested 5 days after selection. Genomic DNA from 1.5 × 106 cells was digested in plugs with MboI and AluI and separated by CHEF gel in the first dimension and by standard 2D gel conditions in the second dimension. DNAs were loaded with partially circularized I × HindIII fragments resulting in comigration in the 2D gel. The blots were probed for the I × HindIII fragments (right), stripped, and reprobed for telomere repeats (left). Arrows in the left bottom panels point to circular telomeric DNA.

Supplemental Table S1. DNA Repair and Checkpoint Genes that Do Not Abrogate TRF2$^{\Delta B}$-Induced Telomere Signal Loss

Cell line	Gene defect	Telomere signal loss
Mouse cell lines		
Immort MEFs	--	30%, 19%
Immort MEFs	ERCC1	18%
Immort MEFs	DNA-PKcs	10%
Immort MEFs	Ku86 (p53)	23%
RH3:E1A	--	44%
RH4:E1A	MSH2	50%
B4:SV40LT	--	43%
B4:SV40LT	MSH2	49%
B4:SV40LT	MLH1	13%
C20, C25	(p53)	32%, 32%
284, 288	Rad51D (p53)	18%, 12%
Human cell lines		
HCT15	Msh6	22%
HCT116	Mlh1	18%
HCT116+chr 3	Mlh1 complemented	13%
AG02496	ATM	17%
AG04405	ATM	19%
BJ/hTERT	--	34%, 43%
BJ/hTERT	+vanillin (DNA-PK inh)	29%, 24%
HeLa	--	19%
HeLa	+vanillin (DNA-PK inh)	27%

Cell lines were infected with TRF2$^{\Delta B}$ and a vector control in parallel and the percentage telomeric signal loss in TRF2$^{\Delta B}$ infected cells compared to the vector control cells was determined as shown in Suppl. Fig. 1 and described in the Experimental Procedures. MEFs were immortalized by introduction of SV40LT, spontaneous immortalization, or due to their p53-/- genotype.

Supplemental Table S1. DNA Repair and Checkpoint Genes that Do Not Abrogate TRF2ΔB-Induced Telomere Signal Loss

Cell lines were infected with TRF2DB and a vector control in parallel, and the percentage telomeric signal loss in TRF2DB-infected cells compared to the vector control cells was determined as shown in Supplemental Figure S1 and described in the Experimental Procedures. MEFs were immortalized by introduction of SV40LT, spontaneous immortalization, or due to their p53-/- genotype.

Supplemental Table S2

Quantitation of TRF2$^{\Delta B}$-induced telomeric signal loss

cell line	retrovirus	chromosomes/ ends scored	signal free ends	chromosomes with two unequal sisters
NIH3T3	vector	784/3136	28 (0.9%)	1 (0.1%)
NIH3T3	TRF2$^{\Delta B}$	706/2824	240 (8.5%)	40 (5.6%)
B4-SV40LT	vector	722/2888	18 (0.6%)	3 (0.4%)
B4-SV40LT	TRF2$^{\Delta B}$	833/3332	133 (4.0%)	38 (4.6%)
MC5	vector	1004/4016	22 (0.5%)	1 (0.1%)
MC5	TRF2$^{\Delta B}$	898/3592	197 (5.5%)	32 (3.6%)
BJ/hTERT	vector	444/1776	10 (0.6%)	1 (0.2%)
BJ/hTERT	TRF2$^{\Delta B}$	448/1792	83 (4.6%)	21 (4.7%)
BJ	vector	392/1568	22 (1.4%)	2 (0.4%)
BJ	TRF2$^{\Delta B}$	416/1664	96 (5.8%)	19 (4.6%)

The indicated cell lines were infected with vector or TRF2$^{\Delta B}$ retroviruses and metaphases were examined in parallel for telomeric signal loss by FISH (as shown in Figure 3A and B). The last column indicates the number of chromosomes that have (partially) lost two telomeric signala, one on each chromosome arm.

Supplemental Table S2. Quantitation of TRF2ΔB-Induced Telomere Signal Loss

The indicated cell lines were infected with vector or TRF2ΔB retroviruses, and metaphases were examined in parallel for telomeric signal loss by FISH (as shown in Figures 3A and 3B). The last column indicates the number of chromosomes that have (partially) lost two telomeric signals, one on each chromosome arm.

References

Bailey, S.M., Cornforth, M.N., Kurimasa, A., Chen, D.J., and Goodwin, E.H. (2001). Strand-specific postreplicative processing of mammalian telomeres. Science 293, 2462–2465.

Cohen, S., and Lavi, S. (1996). Induction of circles of heterogeneous sizes in carcinogen-treated cells: two-dimensional gel analysis of circular DNA molecules. Mol. Cell. Biol. 16, 2002–2014.

Gao, Y., Chaudhuri, J., Zhu, C., Davidson, L., Weaver, D.T., and Alt, F.W. (1998). A targeted DNA-PKcs-null mutation reveals DNA-PK-independent functions for KU in V(D)J recombination. Immunity 9, 367–376.

Karlseder, J., Smogorzewska, A., and de Lange, T. (2002). Senescence induced by altered telomere state, not telomere loss. Science 295, 2446–2449.

Kraakman-van der Zwet, M., Overkamp, W.J., Friedl, A.A., Klein, B., Verhaegh, G.W., Jaspers, N.G., Midro, A.T., Eckardt-Schupp, F., Lohman, P.H., and Zdzienicka, M.Z. (1999). Immortalization and characterization of Nijmegen Breakage syndrome fibroblasts. Mutat. Res. 434, 17–27.

Loayza, D., and De Lange, T. (2003). POT1 as a terminal transducer of TRF1 telomere length control. Nature 424, 1013–1018.

Smogorzewska, A., and de Lange, T. (2002). Different telomere damage signaling pathways in human and mouse cells. EMBO J. 21, 4338–4348.

Takai, H., Smogorzewska, A., and de Lange, T. (2003). DNA damage foci at dysfunctional telomeres. Curr. Biol. 13, 1549–1556.

van Steensel, B., and de Lange, T. (1997). Control of telomere length by the human telomeric protein TRF1 Nature 385, 740–743.

van Steensel, B., Smogorzewska, A., and de Lange, T. (1998). TRF2 protects human telomeres from end-to-end fusions. Cell 92, 401–413.

Zhu, C., Bogue, M.A., Lim, D.S., Hasty, P., and Roth, D.B. (1996). Ku86-deficient mice exhibit severe combined immunodeficiency and defective processing of V(D)J recombination intermediates. Cell 86, 379–389.

Zhu, X.D., Niedernhofer, L., Kuster, B., Mann, M., Hoeijmakers, J.H., and de Lange, T. (2003). ERCC1/XPF Removes the 3¢ overhang from uncapped telomeres and represses formation of telomeric DNA-containing double minute chromosomes. Mol. Cell 12, 1489–1498.